Doctoral thesis

The molecular mechanism for the expression of myosin VI dual function

ミオシン６の２つの生理的機能発現のための分子機構

Keigo Ikezaki

Special Research Promotion Group
Graduate School of Frontier Biosciences
Osaka University

September 2012

概略紹介 (和文)

細胞における力発生を伴う生理機能の多くには、様々な種類の分子モーターが携わっている。ミオシンファミリーはアクチンフィラメントを足場として ATP のエネルギーを用いて力学的な仕事をする分子モーターであり、モータードメイン・レバーアームドメイン・テイルドメインと呼ばれる基本構造を持っている。モータードメインは ATP 加水分解部位およびアクチンフィラメント結合部位を持ち、ATP 加水分解反応と共役させることによりアクチンフィラメントとの親和性およびコンバーター部位(レバーアームとの接続部位)の構造を周期的に変化させている。レバーアームドメインは複数のカルモジュリン結合部位を持ち長く頑強な構造を形成しており、ATP 加水分解反応に伴うモーター部位の局所的な構造変化を増幅している。また、テイルドメインは個々のミオシンファミリーの生体内における活性制御(多量体形成制御、相互作用タンパク質との結合など)に深く関わっている。

古くから研究されているミオシンファミリーのひとつに筋肉の収縮運動に関わるミオシン２がある。ミオシン２は多分子からなるフィラメントを形成し、個々のモータードメインがボートのオールのようにアクチンフィラメントを押すことにより全体として強い力を生み出している。

ミオシン２とは異なる運動機構を持つものとしてミオシン５およびミオシン６が研究されてきた。これらのミオシンは２量体を形成し、２つの力発生部位を交互に前方に押し出すことによりまるで人間の歩行のようにアクチンフィラメント上を移動している(ハンド-オーバー-ハンドモデル)。

ミオシン６の興味深い特徴として細胞内で２つの機械的機能を担っていることが知られている。一つ目はエンドサイトーシスにおける小胞の輸送装置、二つ目はゴルジ体や繊毛などの細胞構造を維持するための固定装置である。私は、ミオシン６が如何にしてこれら２つの機能を両立しているかを理解するために、一分子内二色同時計測法を用いてミオシン６の運動

機構を精査した。歩行中のミオシン6の2つのヘッドドメインの動きの同時計測の結果から、ミオシン 6 はアクチンフィラメントに結合する際に足開きと足閉じの二つの結合状態を取っている事が明らかとなった。また、テイルドメインとヘッドドメインの動きの同時計測の結果から、ミオシン 6 が足閉じ構造を取っているときにレバーアームドメインは安定して前方を向いているということも明らかとなった。これら 2 種類の同時計測の結果から、歩行中の分子全体のダイナミックな動きを明らかにすることに成功した。

私は、先行研究および上記の研究から明らかになったミオシン 6 の運動様式から、ミオシン 6 が外部負荷依存的に輸送装置と固定装置の切替を行っているという動作モデルを提唱した。

GENERAL INTRODUCTION

Various kinds of molecular motors are engaged on most of cellular functions which involve mechanical force, including, but not limited to, cell migrations, mitosis, vesicle transports and maintenances of cellular structures.

Myosin family is one of the actin based molecular motors and they produce mechanical works by using the energy of ATP hydrolysis. Myosins have three basic structural domains; a motor domain, a leaver arm domain and a tail domain. The Motor domain has an actin filament binding site and a nucleotide binding site, and changes the structure of its converter region periodically, which is located at the end of motor domain and connecting to the lever arm domain, coupling with the ATP hydrolysis cycle. The lever arm domain has a number of calmodulin binding sites and forms rigid and long rod structure which enhances the local structural change of converter domain. The tail domain relates to the regulations of indivisual myosin's activities in cell, which include a multimer formation activity and interaction activities between binding proteins.

Myosin II, which is responsible for muscle contractions, is well investigated for a long time. Myosin II forms a filamentary structure with multimer via their long tail domains and each head domain pulls the actin filament like oars of boat resulting in producing large force in all.

Myosin V and VI, which are also well investigated, have a different motion mechanism from myosin II. These myosins form homodimmer and walk along an actin filament by pushing forward their two head domains alternatively like a human's walk (hand-over-hand model).

Myosin VI has an interesting physiological property, namely it's responsible for two

mechanical functions in a cell. One is a transporter for a vesicle transport in an endocytosis process, another is an anchor for maintenance of cellular structures, including, without limitation, Golgi apparatuses and stereocilia. Here, to clarify how myosin VI reconciles its dual function, I investigated its stepping mechanism by performing simultaneous observations of two different colored fluorophores in a single motor protein with nano meter accuracy. These observations revealed the whole molecule dynamics of myosin VI during stepps.

From these results and previous studies, I proposed a working model which myosin VI switches its mechanical roles; a transporter and an anchor, according to environmental situation, including external forces.

<INDEX>

1. Abstract -8-

2. Background -10-

3-1. Experiment 1 -15-

INTRODUCTION 1 -15-

RESULT 1 -16-

Simultaneously Observing Two Myosin-VI Heads Reveals Stepping Pattern of Large and Small Steps.

DISCUSSION 1 -25-

Myosin VI performs three types of steps by taking both the distant and adjacent binding state.

3-2. Experiment 2 -29-

INTRODUCTION 2 -29-

RESULT 2 -32-

Simultaneously observing a myosin VI head and its tail domains.

Coupling of the head and tail domains during motility.

Stability of the lever arm domain during the adjacent binding state.

DISCUSSION 2 -47-

Stepping model for myosin VI.

Forward bias of the lever arm domain.

The adjacent binding state contributes to the myosin VI anchoring function.

4. Conclusion -54-

5. Experimental section -55-

6. References -58-

7. Acknowledges --66

8. Presentation List -67-

1. Abstract

Myosin VI is a universal motor protein that has been identified in organisms ranging from the roundworm Caenorhabditis elegans to humans. It is responsible for many cellular functions including endocytosis, protein secretion, and maintenance of both the Golgi morphology and stereocilia. To achieve these disparate functions, myosin VI must play two different roles: that of transporter, for which myosin VI must move processively, and that of cytoskeletal anchor, for which myosin VI must anchor itself to the actin filament. However, little is known about how myosin VI reconciles its dual function.

Recently, Arimoto and Nishikawa reported that these head-domain steps can be classified into three types: a large step, a small step, and a backward step. Because this stepping mechnism appears unique to myosin VI, it may explain myosin VI's dual function.

Here, in order to clarify how these steps are generated and regulated by the two myosin-VI head domains and its lever arm domains, I here performed simultaneous observation of the myosin VI's two domains (two head domains/ head and tail domains) by labeling the regions with Qdots of different wavelengths, which allowed us to measure the distance between two different colored fluorescent probes with nanometric resolution, or SHREC (Churchman, 2005).

Simultaneous observation of two head domains revealed that myosin VI could take two binding patterns against actin filament; namely a distant binding state, in which the inter-head domain distance is about 34 nm, and an adjacent binding state, in which the inter-head domain distance is less than 10 nm. These two binding state enables myosin VI to take various sizes of steps. Furthermore, this observation also revealed that the successive backward steps are prohibited somehow. Simultaneous observation of myosin

VI head and tail domains revealed that the lever arm is biased forward (the direction of movement) in the adjacent binding state and prohibit successive backward steps from this binding state. From these results and previous studies, we revealed whole stepping scheme of myosin VI and proposed a model to explain how myosin VI achieves its two functions.

2. Background

Myosin VI is a universal motor protein that has been identified in organisms ranging from the roundworm Caenorhabditis elegans to humans. It is responsible for many cellular functions including endocytosis, protein secretion, and maintenance of both the Golgi morphology and stereocilia (reviewed in Sweeney and Houdusse, 2007).

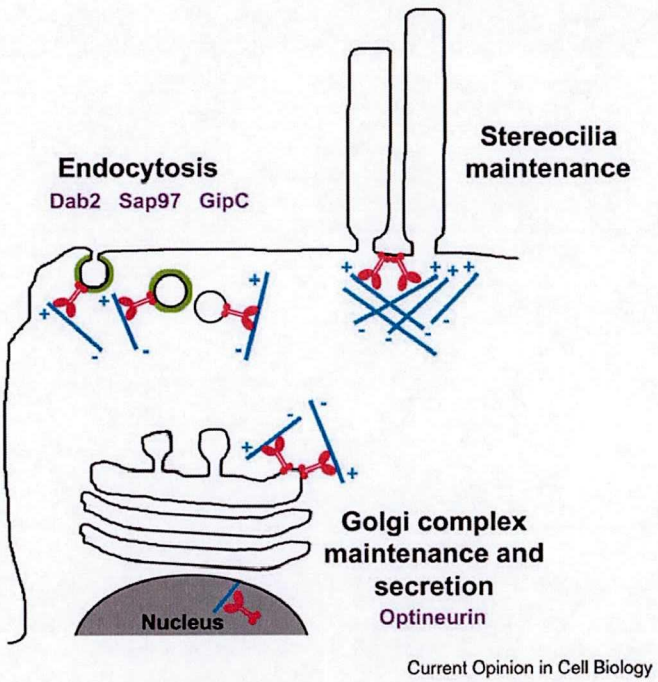

Figure 1 .Cellular functions of myosin VI.

Myosin VI is engaged in many cellular functions. To achieve these disparate functions, myosin VI works as both a transport and an anchor. Myosin VI and actin filament are indicated by red and blue, respectively. The mechanisms by which myosin VI fulfils these functions are largely unknown. (Sweeney and Houdusse, 2007)

The myosin VI heavy chain, like many other myosins, consists of three domains, the head, lever arm and tail. The head is composed of an N-terminal motor domain that consists of

a catalytic domain, which includes the actin and nucleotide binding sites and a converter region. The lever arm domain includes two calmodulin-binding motifs (unique insert and IQ motif) (Bahloul et al., 2004). The tail is composed of four subdomains: the proximal, medial and distal tails, and the C-terminal cargobinding domain. It is also the location where the two heads adjoin to form a dimer, which is the state in which myosin VI inherently functions in cells (Altman et al., 2007; Park et al., 2006; Phichith et al., 2009). While the crystal structure of the head has been solved, the structure of most of the tail remains unknown (Menetrey et al., 2005, 2008).

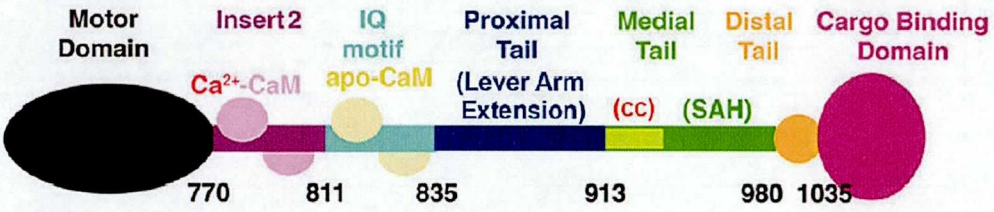

Figure 2. Structural domains of myosin VI.

Myosin VI contains a motor domain (N terminus), followed by a short lever arm containing two calmodulin (CaM)-binding site. This short lever arm is followed by a region that has been referred to as the proximal tail (PT) domain, the medial tail (MT), the distal tail (DT) and finally by the cargo-binding domain (CBD). (Phichith et al., 2009)

As a dimer, myosin VI is a processive motor that moves in a direction opposite that of most other myosins (Bryant et al., 2007; Nishikawa et al., 2002; Park et al., 2007; Rock et al., 2001; Wells et al., 1999). It has short lever arms that include two calmodulin binding motifs and moves processively along actin helical pitches with large step sizes (60–70 nm) (Okten et al., 2004; Park et al., 2006; Yildiz et al., 2004) that are comparable to myosin V despite the latter having much longer lever arms (six calmodulin binding motifs) (Yildiz et al., 2003). In general, the myosin VI stepsize is difficult to reconcile when considering

its short lever arms (Spudich and Sivaramakrishnan, 2010). Most likely, either myosin VI uses an alternative mechanism from the conventional lever arm model, a model frequently applied to other myosins, or its tail domain acts as an extended lever arm. Along with its unexpectedly long stepsize, myosin VI is also distinct in that its step sizes are highly variable (Lan and Sun, 2006; Rock et al., 2001; Sun et al., 2007; Yildiz et al., 2004).

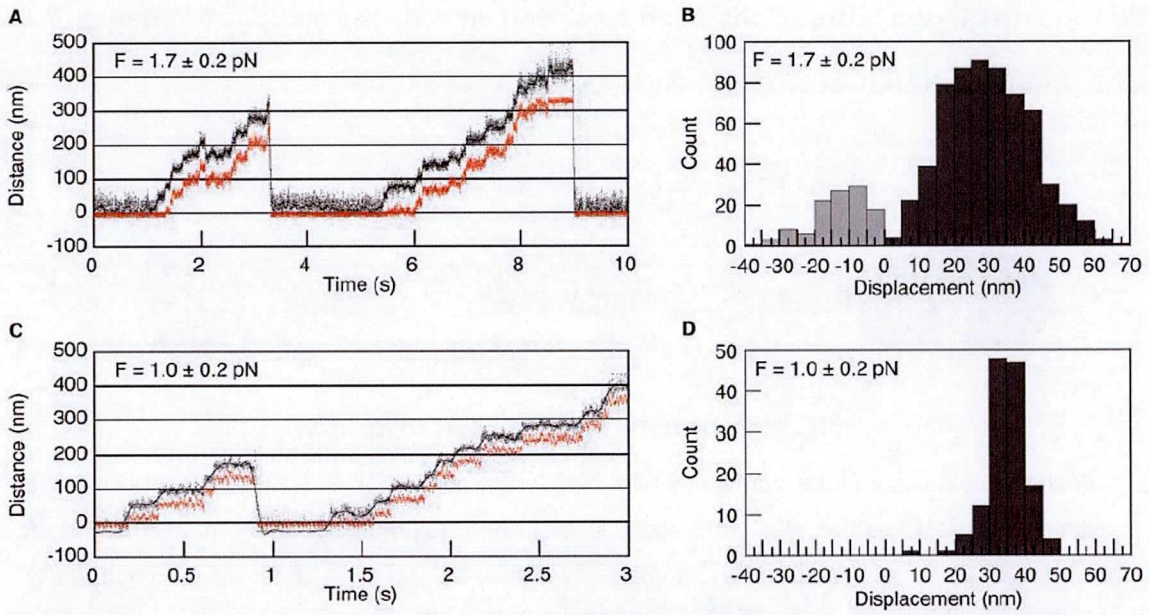

Figure 3. Processive stepping motions and step size distributions of myosin V and VI.

(A, C) Force feedback measurements of single molecule myosin VI and V, respectively. (B, D) Step size distribution of myosin VI and V, respectively, under a backward load. Myosin VI has a significant amount of backward steps and broad forward steps compared to those of myosin V. (Rock et al., 2001)

Spink et al. and Sivaramakrishnan and Spudich have proposed that myosin VI forms a dimer at the cargo binding domain and that its medial tail is a stable a-helix that can act as a relatively rigid extended lever arm (Sivaramakrishnan and Spudich, 2009; Spink et al., 2008). On the other hand, Mukherjea et al. have argued that myosin VI forms its dimer at its proximal and medial tails, the latter consisting of a three-helix bundle in the

monomeric state that upon dimerization subsequently pulls the helix junction to unfold and cause the lever arm to extend in a somewhat flexible manner (Mukherjea et al., 2009). The two models have conflicting limitations. If the extended lever arm is rigid, then the large stepsize can be explained but the broad distribution of stepsizes cannot. In contrast, if the unfolded three-helix bundle is relatively flexible, then the broad distribution of stepsizes can be accounted for but the large stepsizes over a wide range of loads are not (Altman et al., 2004).

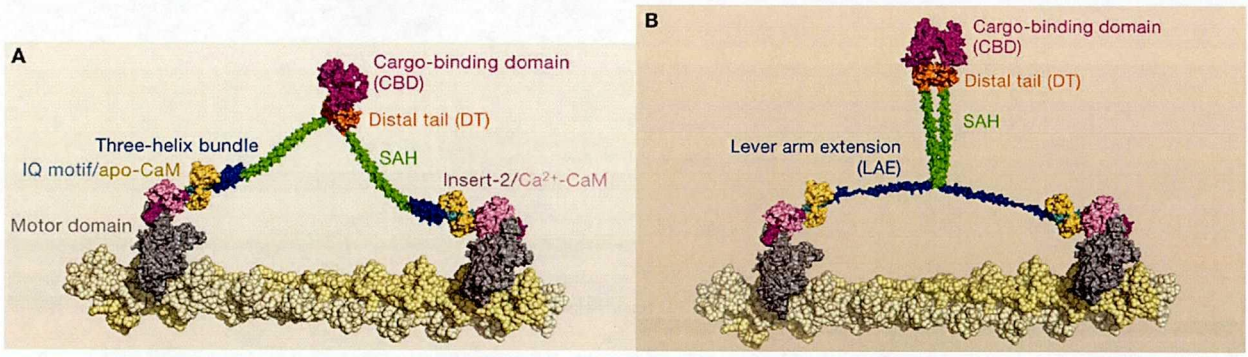

Figure 4. The tail domain structure is still controversial in myosin VI

(A) Model of myosin VI dimer using stable single alpha helices (SAH) as lever arm extensions as proposed by Spink et al. (2008). (B) Model of the dimerized molecule with unfolded three-helix bundle as lever arm extensions. (Sweeney and Houdusse, 2010)

Recently, to further investigate myosin VI's distinctive step behavior, Arimoto and Nishikawa observed myosin VI steps by monitoring quantum dots (Qdots) and gold nanoparticles (GNPs) attached directly to the motor domain, as these offer better spatial and temporal resolutions during single molecule tracking compared to GFP (Balci et al., 2005; Nishikawa et al., 2002; Yildiz et al., 2004). Other groups have used organic fluorescent dyes like Cy3 or Cy5, but attached them to calmodulin bound to an IQ motif, i.e., the lever arm (Okten et al., 2004; Yildiz et al., 2004). Since in these studies the IQ motif is at the distal end of the head, far from the actin binding site, the relative position

of the head to the actin filament could not be ascertained. Along with modifying the labeling molecule, they improved the spatial and temporal resolutions of single molecule nanoimaging by using total internal reflection fluorescence microscopy (TIRFM) and total internal reflection dark field microscopy (TIRDFM). Using these methods, they found two distinct step sizes, one large (72 nm) and one small (44 nm), and the existence of two tilt angles in leading head's lever arm during myosin-VI stepping (Nishikawa et al., 2010).

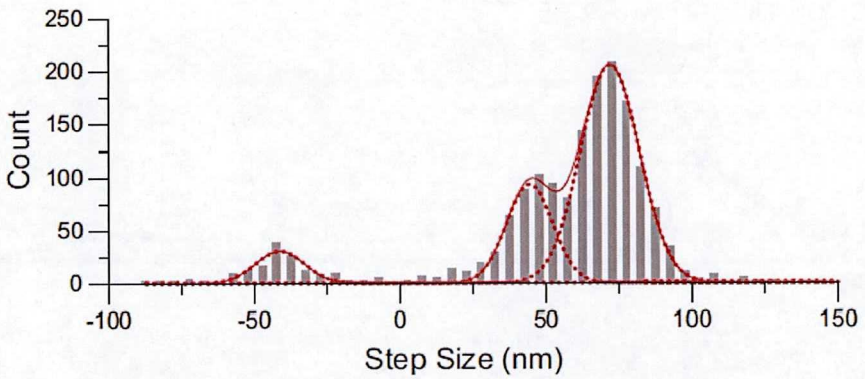

Figure 5. Step size Distribution of a Myosin-VI Head.

Histogram of step sizes at 20 mM ATP. The histogram of step sizes was best fit to a three Gaussian function using a least-squares method (solid and broken lines) with peaks at 71.9 ± 8.9 nm, 43.6 ± 6.9 nm and -41.5 ± 7.0 nm. Myosin VI's forward steps consists of two distinct step sizes. The number of observed steps was 1256. (Nishikawa et al., 2010)

3-1. Experiment 1

INTRODUCTION 1

Arimoto and Nishikawa found two distinct stepsizes in forward steps, one large (72 nm) and one small (44 nm), and the existence of two tilt angles in leading head's lever arm during myosin-VI stepping. Their discoveries clearly indicated that myosin VI's stepping behavior could not be explained by canonical hand-over-hand model.

Here, in order to clarify how the small and large steps are generated by the two myosin-VI heads, I traced its steps by the two heads simultaneously by monitoring differentially-labeled heads with Qdots of different emission spectra using the SHREC method (Churchman et al., 2005). This observation revealed that myosin VI could take two binding patterns against actin filament; namely a distant binding state, in which the inter-head domain distance is about 34 nm, and an adjacent binding state, in which the inter-head domain distance is less than 10 nm. These two binding state enables myosin VI to take small steps. Furthermore, the step rates of the head domains in the adjacent binding state were nearly equal to that of the rear head domain in the distant binding state.

RESULT 1

Simultaneously Observing Two Myosin-VI Heads Reveals Stepping Pattern of Large and Small Steps.

In order to clarify how the small and large steps are generated by the two myosin-VI heads, We traced the steps taken by both head domains simultaneously by labeling them with Qdots of different emission spectra using the SHREC method (see appendix, Churchman et al., 2005) To exclude the possibility that double Qdot labeling disturbed myosin VI motility, we compared its velocity and run length with those of TMR labeled myosin VI (Table 1), finding them to be the same.

Figure 6 shows the time trajectories of the head position. Each head underwent forward (large, 76 ± 9 nm; small, 41 ± 12 nm) and backward steps (-40 ± 13 nm) (Figure 7), similar to the profile seen for single labeled heads (Figure 5) and there is no significant difference between the step size distribution between the two heads (Figure 8). The large forward steps were processive and alternated between the two heads, consistent with the hand-over-hand mechanism (Yildiz et al., 2003). Small steps were also processive, but could not be explained by the hand-over-hand mechanism. No backward steps (out of 280 observations) were observed from the adjacent head binding state.

To clarify the correlation of large, small and backward steps, we analyzed the relationship of two successive steps. Figure 9 shows seven densities in a correlation pattern (pattern I: successive 72 nm and 72 nm steps; pattern II: 72 nm and 44 nm steps; pattern III: 44 nm and 72 nm steps; pattern IV: 44 nm and 44 nm steps; pattern V: 72 nm and -44 nm steps; pattern VI: 44 nm and -44 nm steps; and pattern VII: -44 nm and 44 nm steps). A striking feature in this figure is that there is no density for successive backward steps; backward steps are always followed by small forward steps.

Figure 10 shows a histogram of distances between the two heads after a step was completed. Distance represents the distance between the original leading head and original trailing head such that when the original trailing head leads, distance is negative. The histogram fit to a four Gaussian function with peaks of +35, +10, -7 and -34 nm. The +35 and -34 nm values are consistent with the heads spanning the actin half helical pitch (36 nm), while in myosin V, only a 36 nm distance between the two heads was reported using Qdot labeled myosin V (Warshaw et al., 2005). The +10 and -7 nm values are consistent with the heads being adjacent to each other (adjacent head binding state). The fraction of adjacent head binding state increased in the presence of ADP (data not shown). The feature deduced from the histogram fit to a four Gaussian function is inconsistent with a simplified hand-over-hand model deduced from a histogram fit to a single Gaussian function (Balci et al., 2005). One possible explanation for the disagreeing results is the labels used to determine distance. In the Balci report, eGFP was used. We, however, labeled with Qdot, which is much brighter than eGFP and therefore may explain why we saw two peaks in the two heads distance distribution.

Furthermore, we analyzed the step size distribution after heads took the adjacent binding state (heads separated by less than 15 nm; Figure 11 left) and that after taking the distant binding state (heads separated by over 30 nm; Figure 11 right). Myosin VI produced only small forward steps (45 nm) after the adjacent binding state (Figure 11 left), but took large (75 nm), small (40 nm) and backward (-43 nm) steps at a 1:0.2:0.3 ratio after the distant binding state (Figure 11 right).

Finally, we found the heads alternate between subsequent steps from the adjacent binding state 54% of the time (60/111), which suggests the step rates of both head domains at 100 μM ATP are equal and the step rate of the subsequent steps (2.7 s^{-1}) is

close to that of large steps (2.2 s-1), suggesting both head domains in the adjacent binding state have kinetics that resemble the rear head domain in the distant binding state, namely the post-power stroke state.

	TMR label	Single Qdot label	Double Qdot label
Velocity (mean ± s.d.; μm/s)	57 ± 15 (n=194)	89 ± 28 (n=250)	61 ± 25 (n=150)
Velocity (mean ± s.e.; nm)	227 ± 30 (n=194)	233 ± 34 (n=251)	217 ± 13 (n=150)

Table 1. Run Length and Velocity at 100 μM ATP for Various Labeling Myosin-VI Conditions.

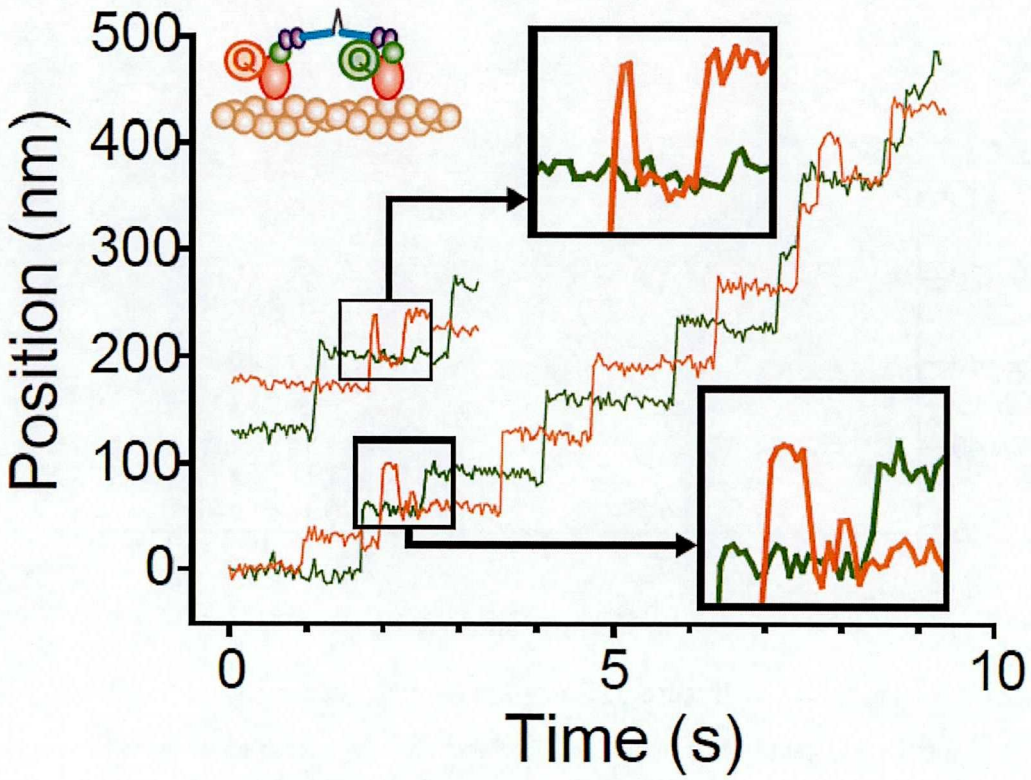

Figure 6. simultaneous observation of myosin VI two head domains

Two head domains were labeled with Qdot525 (green) and Qdot585 (orange), respectively. The colored traces indicate the time trajectory of the head domains at 100 μM ATP. Inserts: magnified traces showing the heads can take the subsequent step from the adjacent binding state with equal probability.

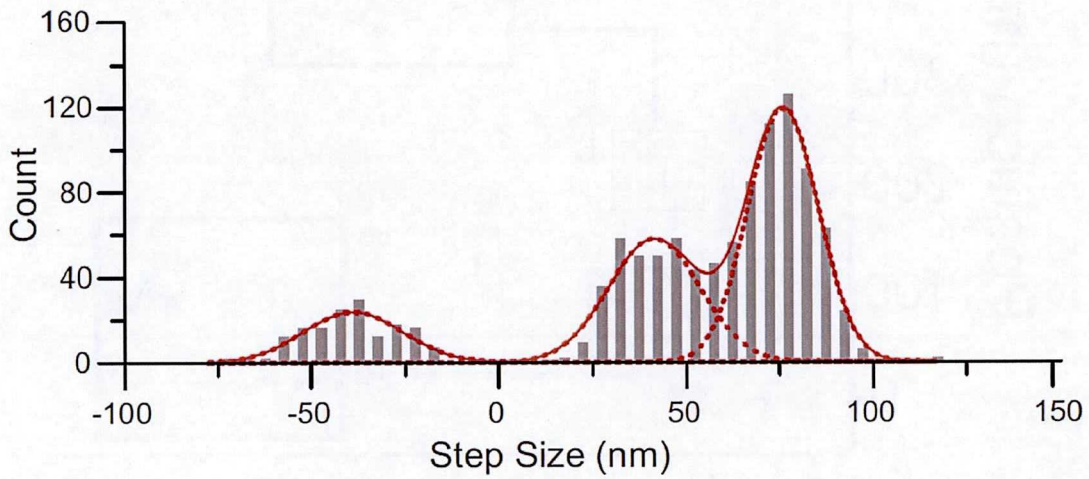

Figure 7. Stepsizes by two heads.

The histogram was best fit to a three Gaussian function using a least-squares method (red solid and broken lines) with peaks of 75.6 ± 7.8 nm, 41.0 ± 10.2 nm and - 39.6 ± 11.0 nm.

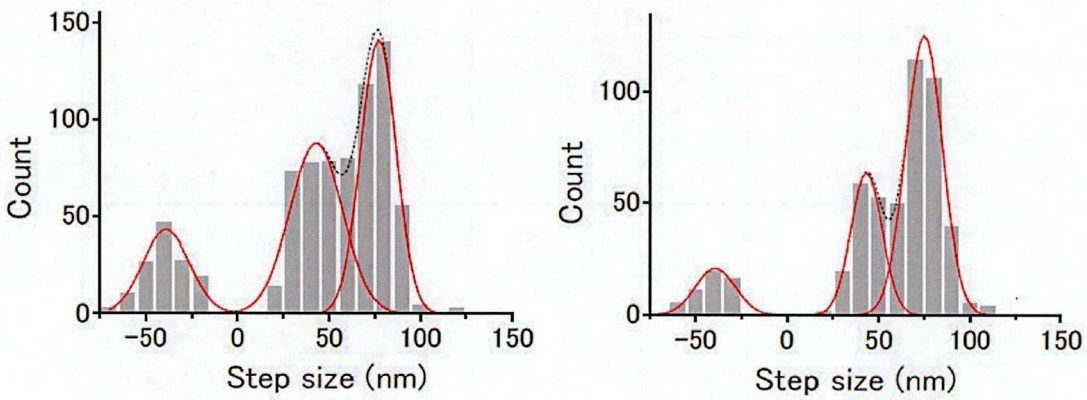

Figure 8. Step size distributions of each colored head domain.

(Left) Step size distribution of the head domain labeled with Qdot525 was fitted with a sum of three Gaussian functions of means ± S.D. -39 ± 11 nm, 43 ± 12 nm and 77 ± 7.9 nm (n= 790). (Right) Step size distributions of the head domain labeled with Qdot585 was fitted with a sum of three Gaussian functions of means ± S.D. -39 ± 9 nm, 43 ± 7.1 nm and 75 ± 8.3 nm (n= 514). There were no significant differences between these two distributions.

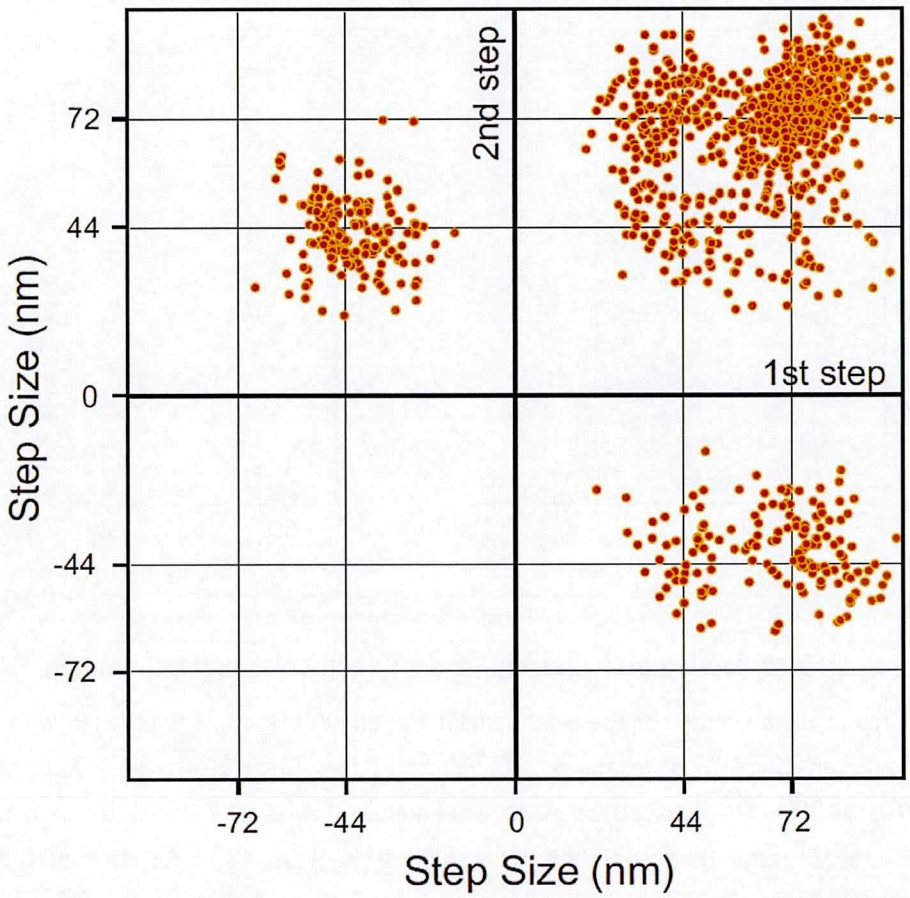

Figure 9. The correlation between two successive steps (n = 1075).

Step size was measured using SHREC observations, meaning all steps, not just those by one head, were observed.

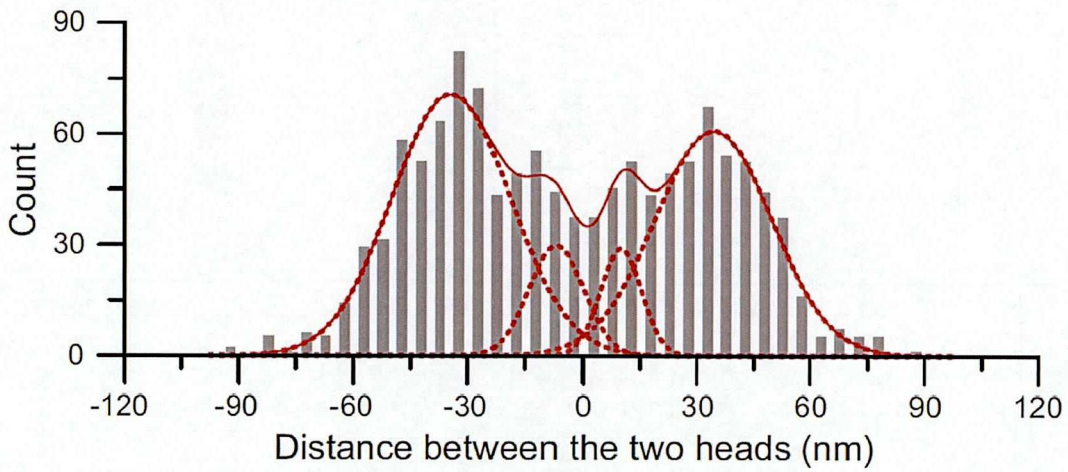

Figure 10. Distances between the positions of the two heads after steps

The histogram was best fit to a four Gaussian function using a least-squares method (solid and broken red lines) with peaks at +34.3 ± 12.8, +9.9 ± 4.3, - 34.5 ± 12.9, and - 6.9 ± 5.8 nm. The number of observed steps was 1219.

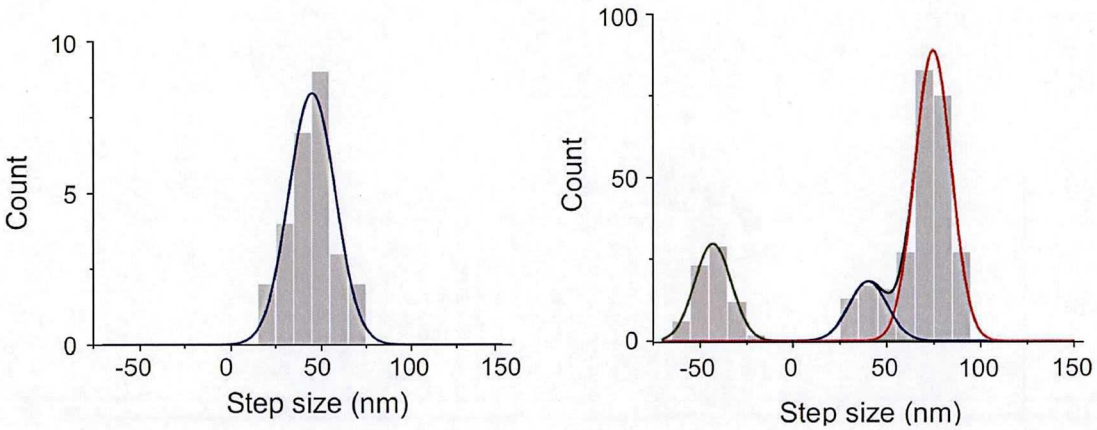

Figure 11. Step-Size Distribution Depending on the Heads-Binding State.

(left) Step size distribution after the adjacent binding state (heads separated by less than 15 nm). Step size distribution was well fit to single Gaussian function with a peak at 45 ± 13 nm. The number of observed steps was 27.

(right) Step size distribution after the distant binding state (heads separated by over 30 nm) was well fit to three Gaussian function with peaks at 43 ± 10 nm, 40 ± 10 nm, 75 ± 8 nm, respectively. The number of observed steps was 330.

DISCUSSION 1

Myosin VI performs three types of steps by taking both the distant and adjacent binding state.

Numerous single molecule assays have contributed to clarifying the myosin-VI stepping mechanism. This has lead to a prevailing model in which myosin VI moves along an actin filament in a hand-over-hand fashion; pushing forward their two head domains alternatively like a human's walk, with a large step size in a manner similar to myosin V, another processive myosin (Nishikawa et al., 2002; Okten et al., 2004; Rock et al., 2001; Yildiz et al., 2004). However, recently, Arimoto and Nishikawa revealed myosin VI has three step sizes and this discovery clearly indicated that myosin VI's stepping behavior could not be explained by canonical hand-over-hand model. Our simultaneous observation of myosin VI two head domains revealed that myosin VI is able to take two binding states against an actin filament (Figure 12). These two binding states enable myosin VI to perform various types of steps (Figure 13 left four schemes). However, successive backward steps from the adjacent binding state are prohibited somehow (Figure 13 right scheme). Furthermore, this observation also revealed that either head domain can take the subsequent small step from the adjacent binding state with equal probability and that the step rate is the same as that for large steps. This result indicates that the structural state of the head domains in the adjacent binding state should be the same as that of the rear head domain in the distant binding state (post-power stroke state). A possible physiological consequence of such a structure is that it facilitates myosin VI ability to avoid intracellular obstacles while acting as a vesicle transporter such that myosin VI can shift its stepping pitch by as much as the length of its head domain, enabling efficient processive movement through a crowded intracellular

environment (Sivaramakrishnan and Spudich, 2009).

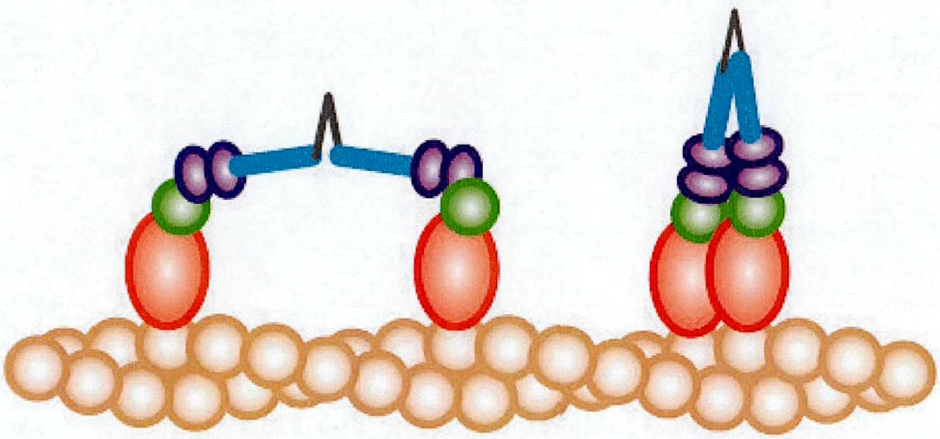

Figure 12. Two types of binding states of myosin VI against an actin filament.

Myosin VI could take two binding patterns against an actin filament; namely a distant binding state, in which the inter-head domain distance is about 34 nm, and an adjacent binding state, in which the inter-head domain distance is less than 10 nm.

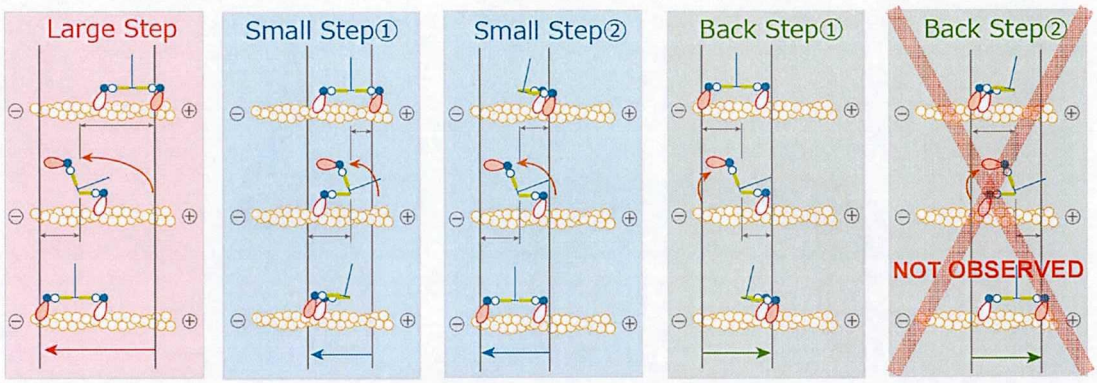

Figure 13. Model for myosin VI Steps

According to the results of simultaneous observation of myosin VI two head domains and previous studies which done by Arimoto and Nishikawa, I proposed myosin VI' s stepping model. Left is large hand-over-hand steps; second and third from the left are small inchworm-like steps from the distant binding state and the adjacent binding state, respectably. Second from the right is backward inchworm-like step from the distant binding state. Right is backward inchworm-like step, but its not observed.

3-2. Experiment 2

INTRODUCTION 2

Myosin VI is a distinct myosin protein responsible for various cellular functions including endocytosis, protein secretion, and maintenance of both the Golgi morphology and stereocilia (Figure 1, Sweeney and Houdusse, 2007). To achieve these disparate functions, myosin VI must play two different roles: that of transporter, for which myosin VI must move processively, and that of cytoskeletal anchor, for which myosin VI must anchor itself to the actin filament.

Mechanically, myosin VI takes forward steps of a wide distribution size and an unusually high number of backward steps (Okten et al., 2004; Park et al., 2006; Yildiz et al., 2004). Recently, Arimoto and Nishikawa reported that these head-domain steps can be classified into three types: a large step, a small step, and a backward step and that the step type is determined by the direction of the lever arm at the beginning of the Brownian search (Nishikawa et al., 2010). Furthermore, I revealed that these three step types were attributed to two binding states: a distant binding state, in which the inter-head domain distance is about 34 nm, and an adjacent binding state, in which the inter-head domain distance is less than 10 nm (Figure 14).

Because the adjacent binding state appears unique to myosin VI, it may explain myosin VI's dual function. However, little is known about the structure of this state, especially the direction of the lever arms, that is whether the two heads take the pre- or post- power stroke state. Therefore, we here performed simultaneous observation of the myosin VI head and tail domains by labeling the regions with Qdots of different wavelengths, which allowed us to measure the distance between two different colored fluorescent probes with

nanometric resolution, or SHREC (see appendix, Churchman, 2005). We found that the lever arm is biased forward (the direction of movement) in the adjacent binding state. From these results, we propose a model to explain how myosin VI achieves its two functions.

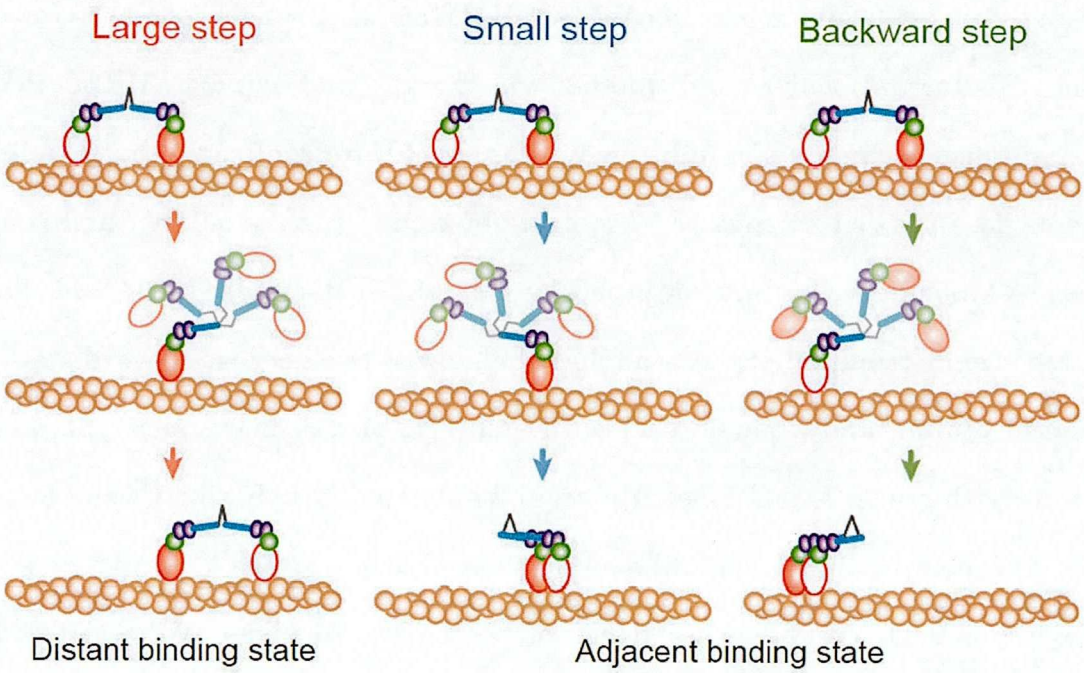

Figure 14. Three step types of myosin VI.

Myosin VI generates three step types by taking either a distant binding or adjacent binding state.

RESULT 2

Simultaneously observing a myosin VI head and its tail domains

To clarify how the tail domain moves during stepping, we labeled the head domain with streptavidin coated Qdot525 via HaloTag and HaloTag-Biotin-Ligand and the tail domain with anti-His-tag-antibody coated Qdot585 via His-tag, and applied SHREC to observe the domain displacements simultaneously (Figure 15). We confirmed that labeling with two Qdots does not disturb myosin VI motility by comparing the velocity and run length to myosin VI labeled with a smaller probe, Tetramethyrhodamine (TMR) (Table 2).

The step size distribution of the head domain showed two distinct forward step sizes of 40 nm and 68 nm, and a single backward step size of -38 nm (Figure 16), which are consistent with single Qdots labeled myosin VI's stepping behavior (Nishikawa et al., 2010) . On the other hand, the tail domain showed only a single forward step size of 35 nm (Figure 17). The very low frequency of the backward steps of the tail domain is consistent with a previous report in which single molecule motility assays were performed under the no load condition,(Elting et al., 2011; Park et al., 2007) whereas backward load applied by an optical trap increases the frequency.(Rock, 2001)

These results demonstrate that the two domains were successfully and specifically labeled with Qdot525 and Qdot585, respectively, and also suggest that our labeling method does not affect the motor activity of myosin VI.

	TMR label	Double Qdot label (Head and Tail)
Velocity (nm/s) (mean ± s.d.)	17.7 ± 4.5	25.2 ± 8.2
Run length (nm) (mean ± s.e.)	151 ± 8.6	197 ± 3.5

Table 2. Run length and velocity at 20 μM ATP for different labeling myosin VI conditions.

Run length at 20 μM ATP was determined by fitting each distribution to a single exponential decay function. Velocity at 20 μM ATP was determined by fitting each distribution to a Gaussian function. There is not much difference between labeling conditions, indicating any Qdot labeling effects on myosin VI stepping were independent of the Qdot. The numbers of analyzed traces for TMR labeled myosin VI and double Qdot labeled one are 1016 and 294, respectively.

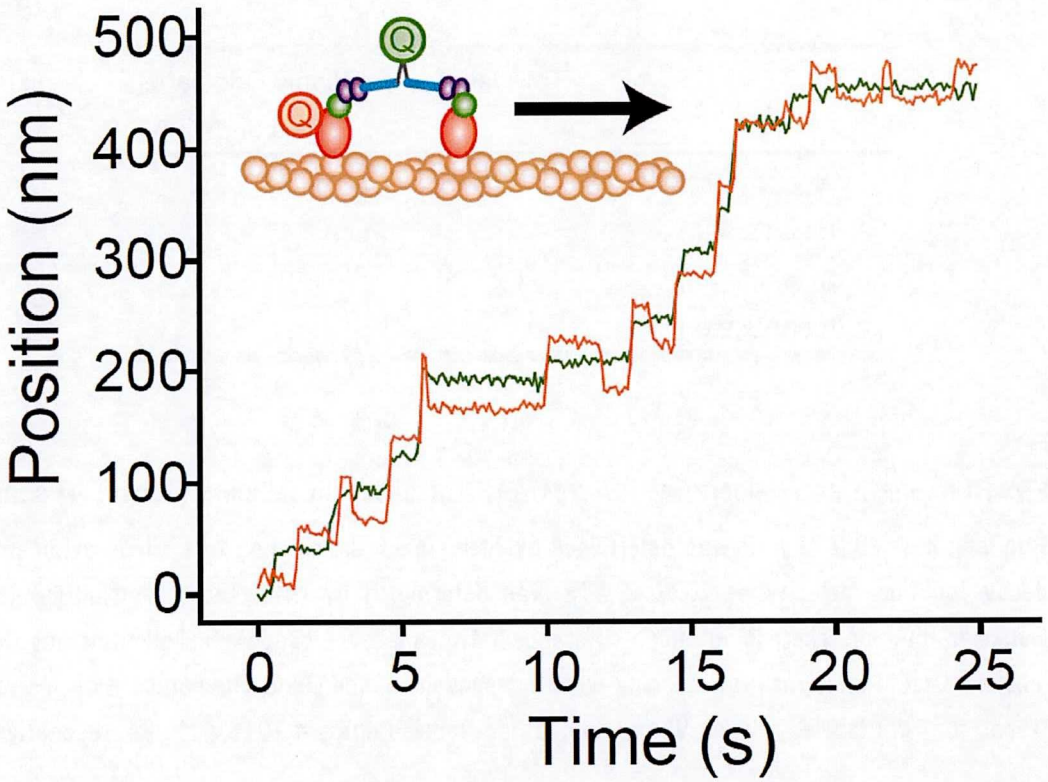

Figure 15. Simultaneous observation of myosin VI head domain steps and tail domain displacements.

Time trajectory of myosin VI head domain steps (orange) and tail domain displacements (green) at 20 μM ATP.

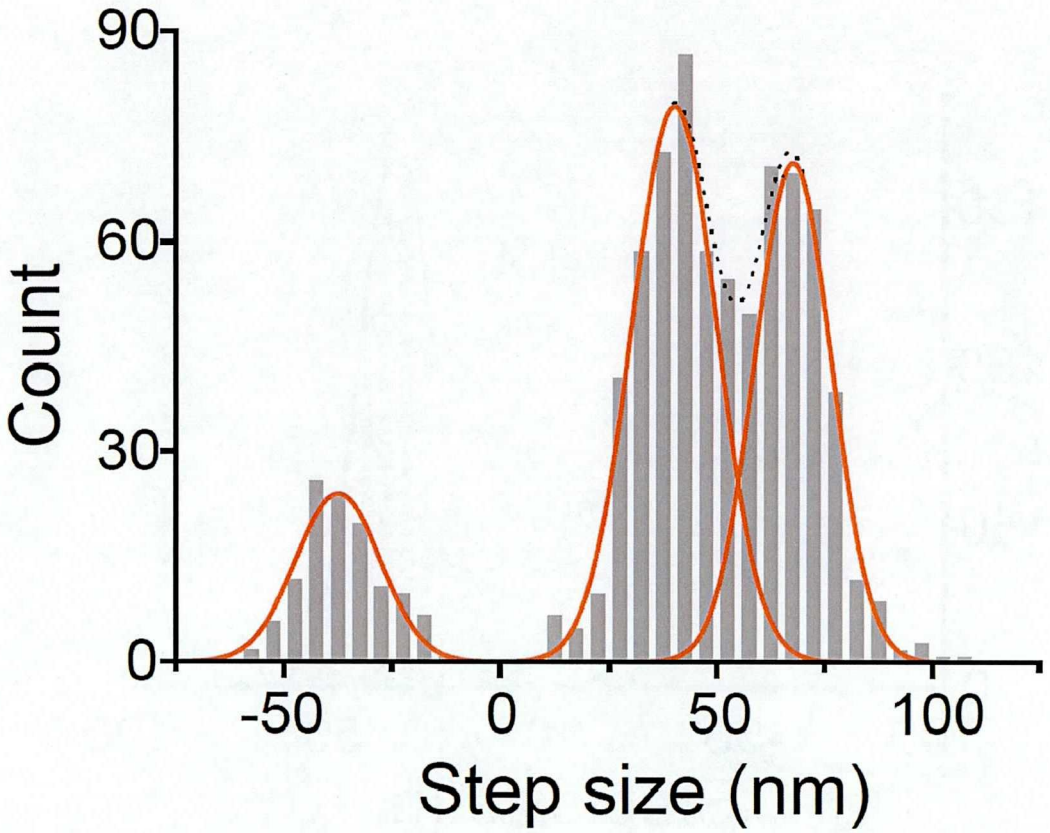

Figure 16. Histogram of the distribution of myosin VI head domain steps at 20 μM ATP.

The distribution was fitted with a three Gaussian function of means ± S.D. 68 ± 7.2 nm, 40 ± 8.1 nm and -38 ± 8.0 nm.

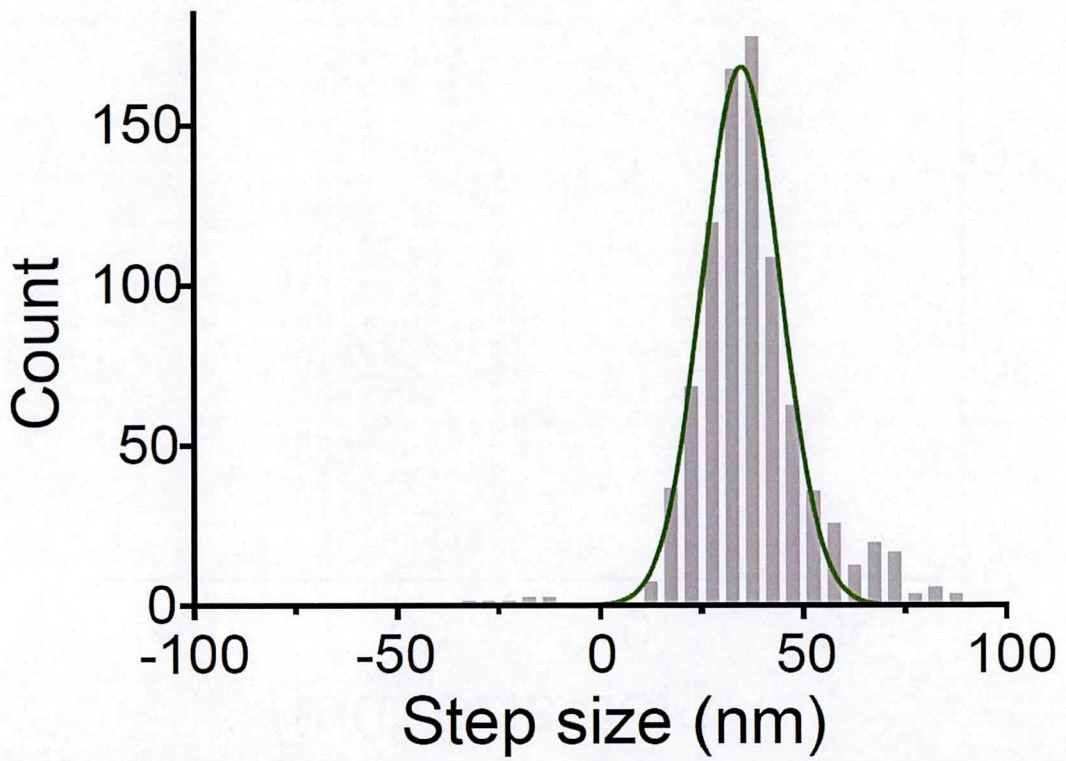

Figure 17. Histogram of the distribution of myosin VI tail domain displacements at 20 μM ATP.

Step size distribution was fitted with a Gaussian function of mean ± S.D. 35 ± 7.8 nm.

Coupling of the head and tail domains during motility

To clarify how tail domain movement couples with the three types of myosin VI head domain steps, we analyzed the tail domain positional change at the time of each head domain step by subtracting the mean value of the tail domain position before a head domain step from that after the step (Figure 18-20). To minimize aliasing caused by the next step of the unlabeled head, we analyzed only three tail domain positions before and after a head domain step, respectively (-300, -200, -100 ms and 100, 200, 300 ms, respectively).

The distribution of the tail domain movement during large head-domain steps was fitted to a single Gaussian function with a mean of 27 nm (Figure 18). This value is comparable to the distance between two heads in the distant binding state and indicates the tail domain always moves with a large head-domain step. That the 27 nm value is less than the 34 nm expected from a 68 nm hand-over-hand step, is caused by the sensitivity of our calculation to the rising phase of the tail displacements (Figure 22). Figure 2B shows that the head and tail domains coupled during a head-domain step, which is consistent with the canonical hand-over-hand model.

In the case of small head-domain steps, the distribution of tail domain movement was fitted to a sum of two Gaussians function with means of -0.2 nm and 27 nm (Figure 19). As in the case of the large head-domain step (Figure 18), the 27 nm distribution for the small step shows coupling between the tail and head domain movements (Figure 19, center). On the other hand, the -0.2 nm value indicates that the tail domain does not move appreciably during small head-domain steps (Figure 19, right).

To clarify the timing of the lever arm swing during small head-domain steps, we next examined time lags between the tail domain movement and the previous small step of the

head domain. The distribution of the time lags was fitted to a sum of two exponential decays function with means of 0.06 s and 0.6 s (Figure 21). The 0.06 s constant suggests these tail domain displacements coupled with small head-domain steps within our sampling rate (0.1 s). In contrast, 0.6 s is consistent with a myosin VI head's stepping dwell time of 0.76 s at 20 μM ATP, suggesting these tail domain movements couple to the subsequent head-domain steps.

Finally, the distribution of tail domain movement during backward head-domain steps was fitted to a single Gaussian function with a mean of 2.9 nm (Figure 20). Such a small value indicates that tail domain movements do not couple with backward head-domain steps (Figure 20).

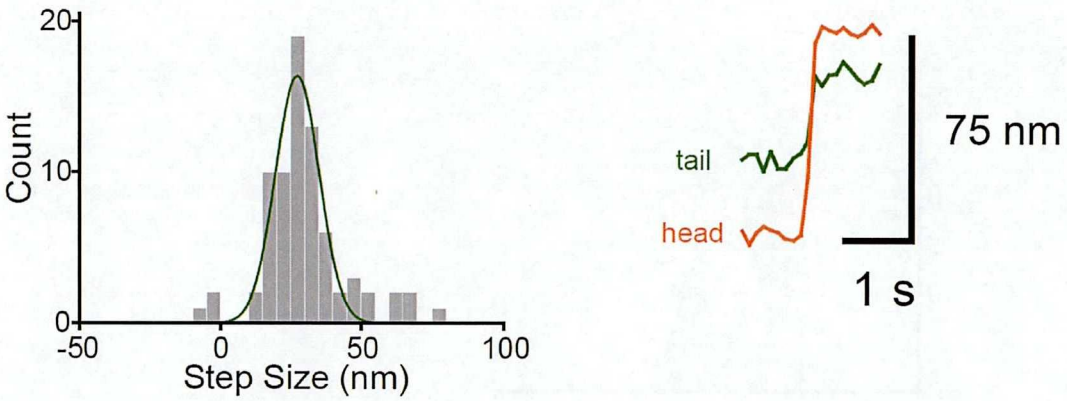

Figure 18. Tail domain displacements coupled to large steps of the head domains.

We analyzed tail domain positional change at the time of the large step of the head domain by subtracting the mean value of three positions before a head domain step from that after the step. Tail domain displacements coupled to large steps. Step size distribution was fitted with a single Gaussian function of mean ± S.D. 27 ± 6.4 nm (n= 75). Magnified time trajectory is typical one showing coupling between a head domain large step (orange) and tail domain displacement (green).

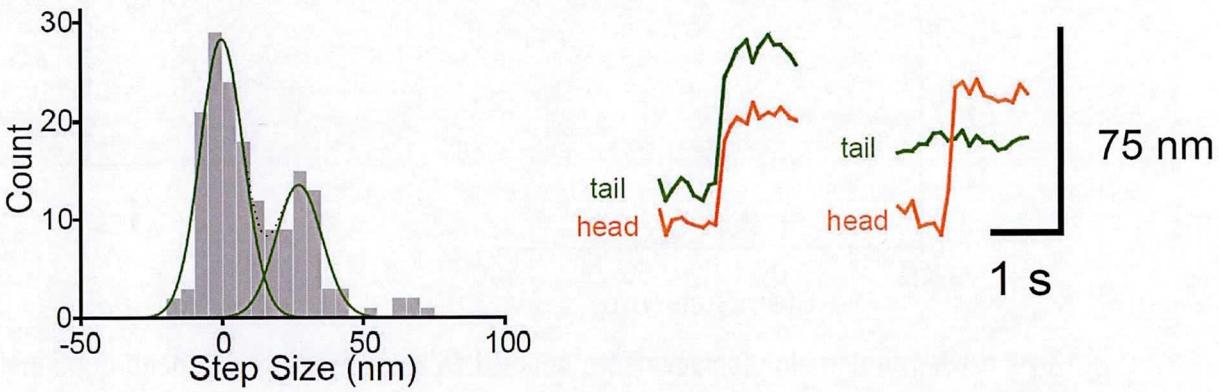

Figure 19. Tail domain displacements coupled to small steps of the head domains.

We analyzed tail domain positional change at the time of the small step of the head domain by subtracting the mean value of three positions before a head domain step from that after the step. Tail domain displacements coupled to small steps. Step size distribution was fitted with a sum of two Gaussian functions of means ± S.D. -0.2 ± 6.3 nm and 27 ± 6.7 nm (n= 167). Magnified time trajectories show coupling (left) and non-coupling (right) between head domain small steps (orange) and tail domain displacements (green).

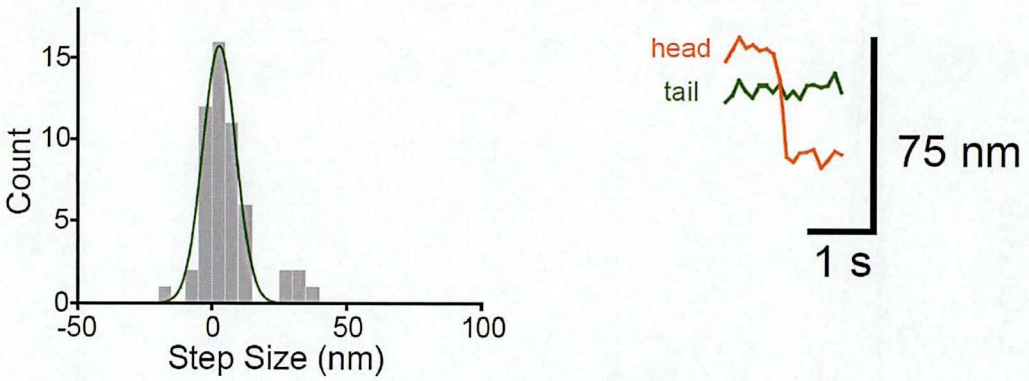

Figure 20. Tail domain displacements coupled to large steps of the head domains.

We analyzed tail domain positional change at the time of the backward step of the head domain by subtracting the mean value of three positions before a head domain step from that after the step. Tail domain displacements coupled to head domain backward steps. Step size distribution was fitted with a single Gaussian function of mean ± S.D. 2.9 ± 5.0 nm (n= 53). Magnified time trajectory showing non-coupling between a head backward step (orange) and tail domain displacement (green).

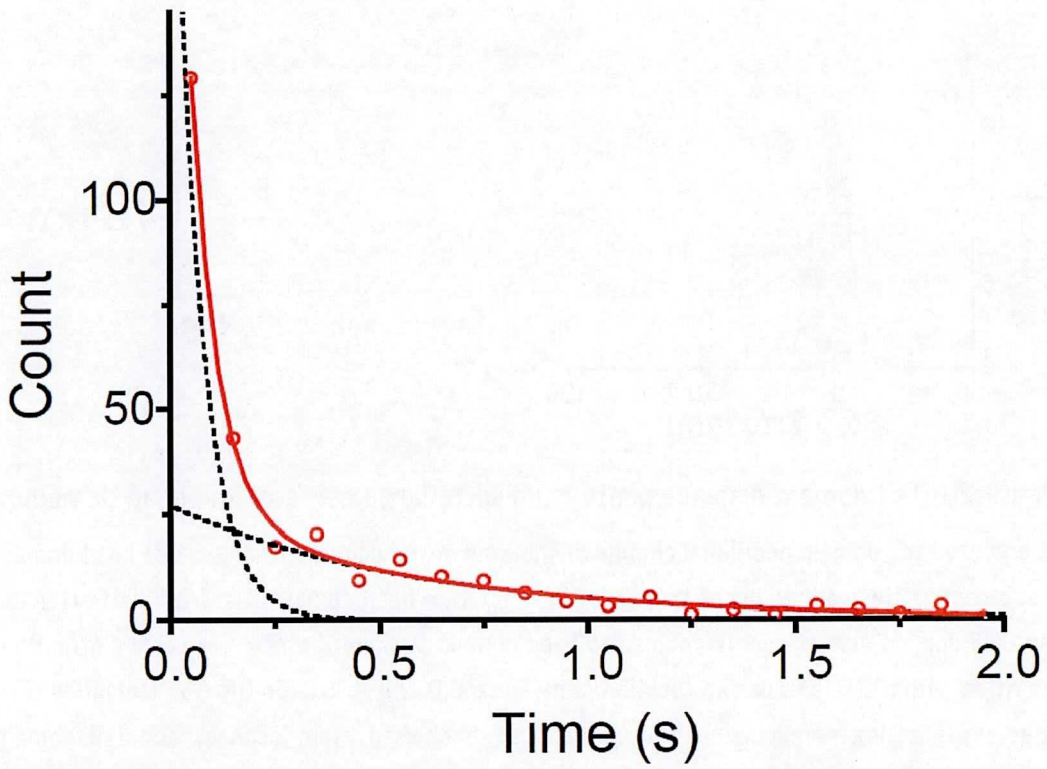

Figure 21. Distribution of time lags between the tail and head domain movement.

Distribution of time lags at 20 μM ATP was fitted to a sum of two exponential decays function with means of 0.06 s and 0.6 s. The number of observed steps was 287.

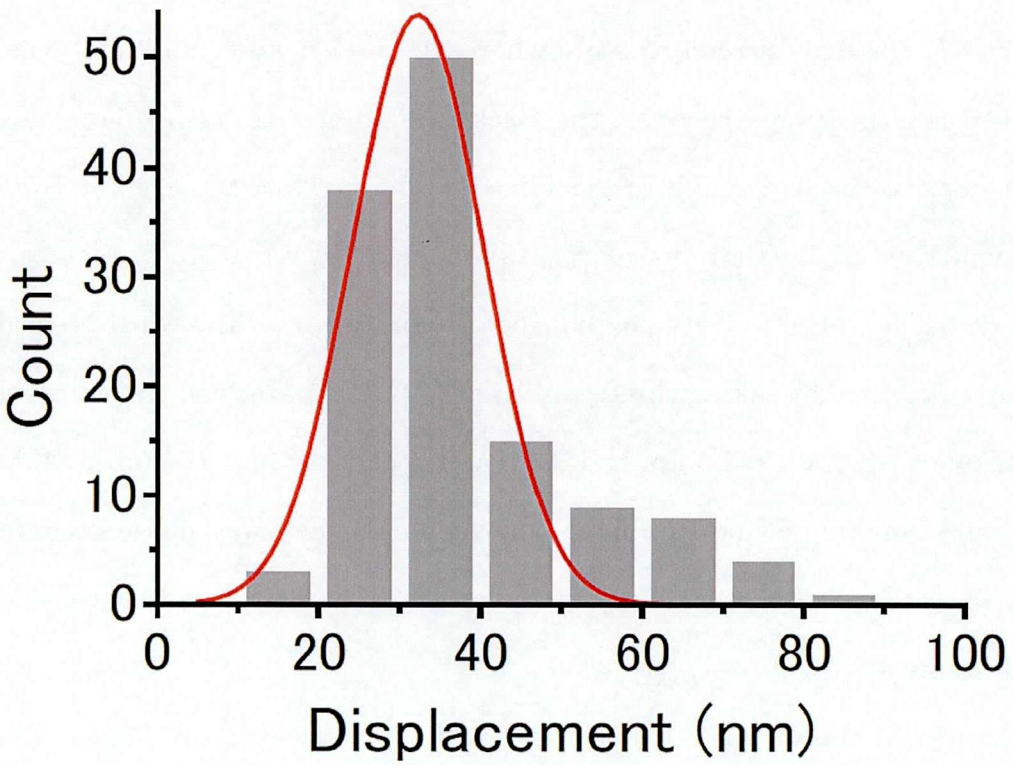

Figure 22. Tail domain movements during head domain large steps.

In Figure 18, we calculated tail domain displacement by subtracting the mean value of three tail domain positions before a head-domain step (-300, -200, -100 ms) from that after the step (100, 200, 300 ms). This method, however, is sensitive to the rising phase of the tail displacements. To reduce this affect, we calculated tail domain displacements using all points in the dwell time. The distribution of the tail domain movement during large head-domain steps was fitted to a single Gaussian function with a mean of 32 nm, which approximates the 34 nm expected from a large step of 68 nm (Figure 17).

Stability of the lever arm domain during the adjacent binding state

Simultaneous observation of myosin VI two head domains revealed that backward steps occur only after the distant binding state where the inter-head domain distance is 34 nm (Figure 14). Furthermore, because the backward step size is -38 nm (Figure 16), backward steps necessarily result in the adjacent binding state (Figure 23). Knowing this, we can evaluate the fluctuations of the tail domain in each binding state from the standard deviations (S.D.) of its position before and after a backward step. The S.D., which were calculated by taking three points of the tail domain time trajectory before and after a backward step, were 4.3 nm and 3.9 nm, respectively (n = 77, Figure 23). That the two S.D. were similar and no significant movement of the tail domain occurred during backward steps (Figure 20) suggests that the lever arm domains tilt forward stably in the adjacent binding state.

We also analyzed the distance between the tail and head domain during the adjacent binding state (Figure 24). The distribution of the distances was fitted to a single Gaussian function with a mean of 26 nm, suggesting that no-lever arm compression occurs during the adjacent binding state.

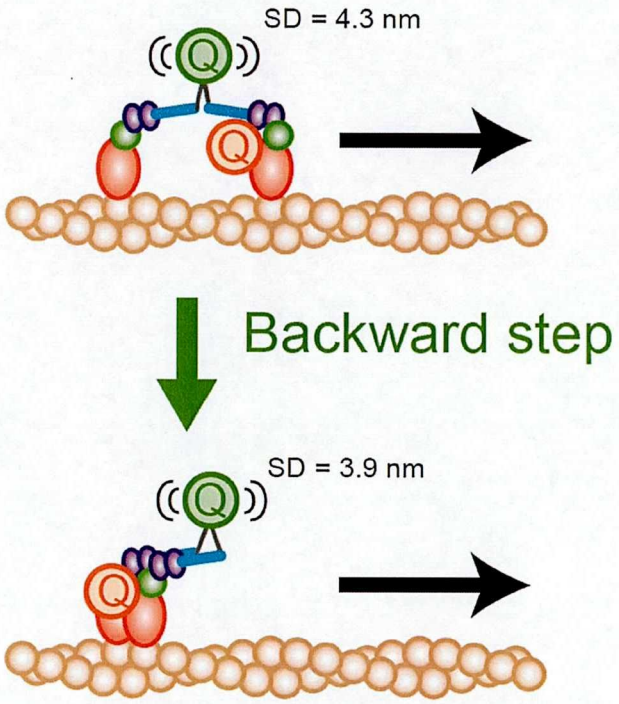

Figure 23. Fluctuations of the tail domain in each binding state.

In the distant binding state (upper), the two heads bind to an actin filament with a distance of about one actin filament half pitch. In the adjacent binding state (lower), they bind next to each other. The standard deviations (S.D.) of the tail domain position before and after a backward step were 4.3 nm and 3.9 nm, respectively (n = 77).

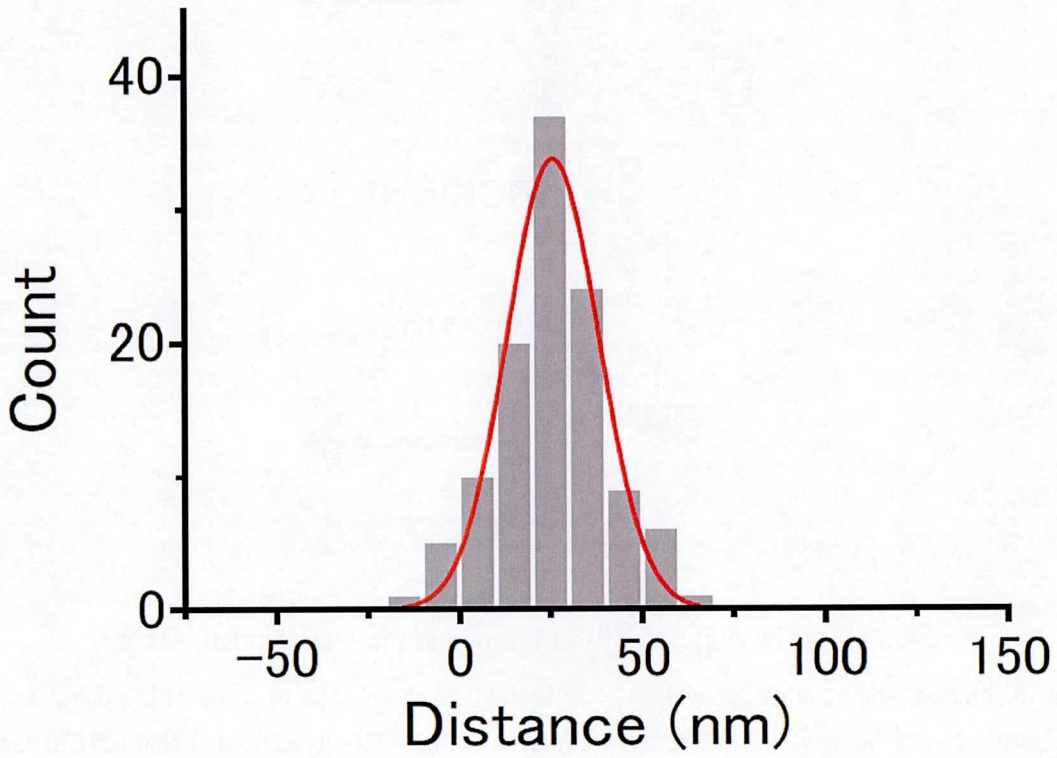

Figure 24. The distance between the tail and head domain during the adjacent binding state

The distance between the tail and head domain during the adjacent binding state were calculated by subtracting the mean value of three positions of the tail domain from that of the head domain at 100, 200, and 300 ms after the head-domain backward step in individual traces. The distribution of the distances was fitted to a single Gaussian function with a mean of 25.7 nm (n = 113). Because Qdots were attached behind the center of the head domain, the distance is larger than the expected leaver arm domain length (see Figure 23, lower cartoon).

DISCUSSION 2

Stepping model for myosin VI

In this study, we show that the lever arm swings coupled to small head-domain steps (Figure 19). Considering our previous study in which we reported that the lever arm domain does not swing during the Brownian search, in which state myosin VI binds to actin filament with a single head domain and the other head searchs the next binding site using thermal fluctuation of water molecules, of small steps, (Nishikawa et al., 2010) these lever arm swings should occur almost instantly after a small step. Furthermore, we revealed that the lever arm domain of the binding head maintains the forward tilt during backward steps (Figure 20) and that the lever arm domains tilt forward stably in the adjacent binding state (Figure 23, 24). Taken together, we propose a comprehensive scheme for myosin VI stepping motion (Figure 25). The scheme indicated by Figure 25 A →B→C corresponds to the large steps shown in Figure 18. The two types of small steps (Figure 19, center and right) correspond to the schemes in Figure 25 A→D→E→F and Figure 25 F→B→C, respectively. Backward steps in Figure 20 correspond to the scheme shown in Figure 25 A→G→F. Furthermore, lever arm swings immediately occur after taking the adjacent binding state during small steps (Figure 25 E→F) and lever arm domains tilt forward stably in the adjacent binding state (Figure 25F), as mentioned above.

Recently, two groups have proposed structural models for the myosin VI in the distant binding state (Figure 4, Mukherjea et al., 2009; Spink et al., 2008). Although the details of these two models, especially the lever arm structures, are controversial, both studies proposed that myosin VI dimers have an unexpectedly long and stable lever arm during

processive movement that becomes compact when myosin VI is a monomer. In this respect, our results are consistent with these two structural models, especially in the distant biding state. Although the detailed structure of the adjacent binding state remains unclear, our study reveals that the lever arms in the adjacent binding state takes the extended conformation, not the compact conformation of the monomer state.

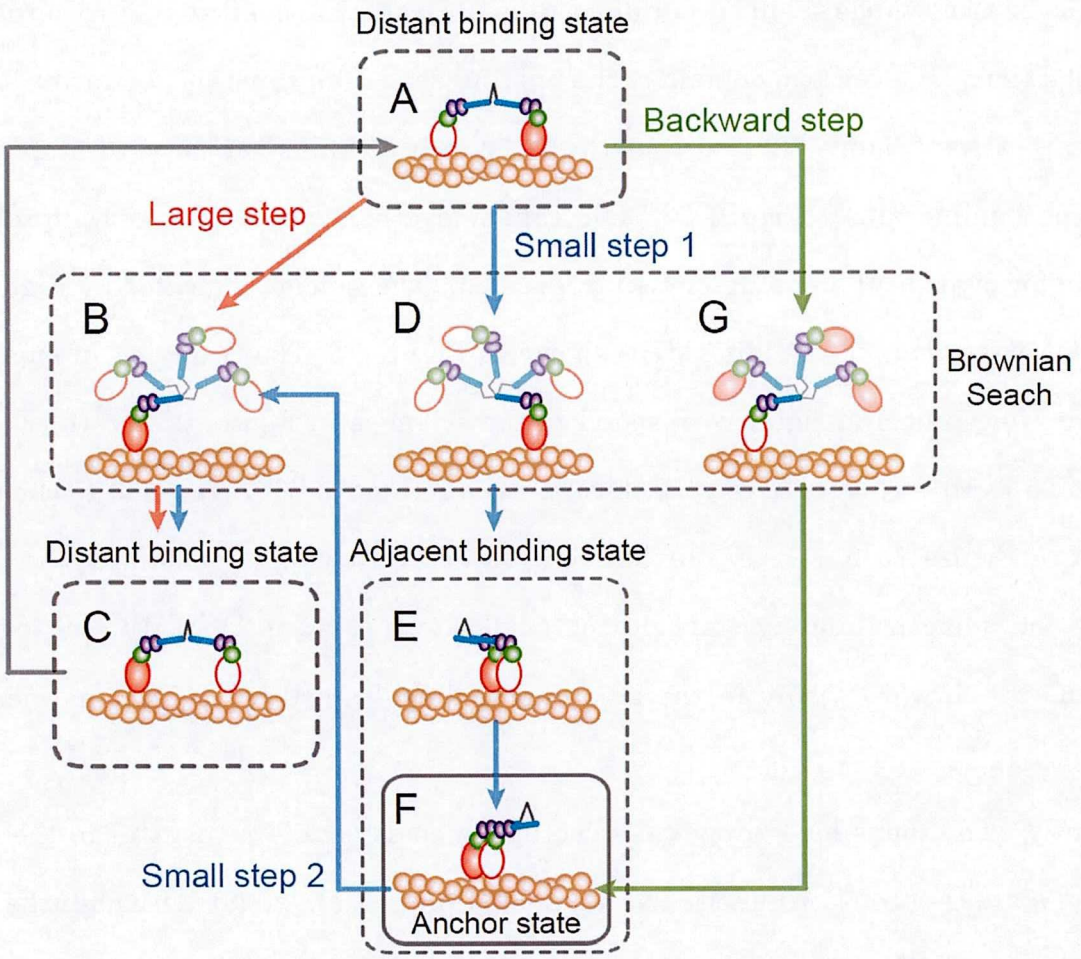

Figure 25. Model for myosin VI steps.

(See next page)

Figure 25. Model for myosin VI steps.

A model for myosin VI steps. Large steps are generated in accordance with the hand-overhand mechanism. Initially, the head domains are in the distant binding state in which their distance apart approximates the half actin helical pitch (A). Next, the trailing head domain detaches from the actin filament upon ATP binding (B), rebinding at the subsequent forward actin target 68 nm away (C). During this time, the tail domain moves 27 nm forward (about one actin half helical pitch), coupling with the head domain movement. Small steps are generated in two ways. In one, they arise from the distant binding state (A). Upon detaching by ATP binding, the trailing head domain performs a Brownian search (D) and rebinds 40 nm forward, resulting in the adjacent binding state (E). The lever arm swing occurs immediately after rebinding of the detached head domain (F). In the other, small steps arise from the adjacent binding state (F). Here, one head domain detaches from the actin filament upon ATP binding (B) and rebinds 40 nm forward, resulting in the distant binding state without a lever arm swing (C). Backward steps can only occur from the distant binding state (A). The leading head domain detaches from the actin filament (G) and rebinds 38 nm backward (F). No lever arm swing occurs during a backward step. According to this model, when an unlabeled head domain performs a large step (A→B→C) or a small step 1 (A→D→E→F), we should observe a tail domain displacement without a labeled head domain displacement, a phenomenon we observed (Figure 15, e.g. around 1 sec)

Forward bias of the lever arm domain

The fact that the tail domain does not move during backward steps indicates that the lever arm domains tilt forward in the adjacent binding state, with both head domains in a post-power stroke state. Furthermore, no significant differences in tail domain fluctuations between the adjacent binding and distant binding state suggests both heads stably retain the post-power stroke state during the adjacent binding state. This preferential forward tilting of the lever arm domain during backward steps is consistent with previous biochemical experiments, which reported that the rear head of myosin VI takes either the ADP-binding or no nucleotide binding state,(De La Cruz, 2001) and crystal structure analyses, which reveal that the lever arm tilts forward with no nucleotide and ADP binding state.(Ménétrey et al., 2005; Ménétrey et al., 2007) Furthermore, given our hypothesis that the structural state of the head domains in the adjacent binding state is the same as that of the rear head domain in the distant binding state (discussed in Experiment 1), the preferential forward tilting of the lever arm domain in the adjacent binding state is also a consistent result. In the presence of a backward load of up to a stall force, we assume that myosin VI tends to take the adjacent binding state and its lever arms tilt forward. This is supported by a report showing that the tail domains rarely swing backwards even under a backward load of up to 2 pN,(Chuan et al., 2011) which would not be the case if they were flexible. When a stall force, over which myosins detach from the actin filament, is applied to the tail domain, the lever arm is seen to frequently swing backwards.(Rock, 2001) These oscillations were likely independent of ATP binding because of their unusually high rates. Assuming that the oscillations are not coupled with dissociation and rebinding of the head domain, the oscillations should represent a transition between pre- and post-power stroke states due

to excessive backward loads in the adjacent binding state.

The adjacent binding state contributes to the myosin VI anchoring function

The adjacent binding state should be ideal for myosin VI to equally divide any external load onto both its head domains. This is unlike the distant binding state where a disproportionate amount of force is applied onto the leading head. Such kinetics could also help prevent spontaneous detachment. It has been reported that in myosin V, another processive myosin, the front head domain, in which the structural state is the pre-power stroke state, spontaneously detaches from the actin filament at a rate of 1 s^{-1} (Purcell et al., 2005) and that the binding strength of the front head domain is weaker than that of the trailing head domain.(Gebhardt et al., 2006) Because in the adjacent binding state both myosin VI heads are in the post-power stroke state, such spontaneous detachment should not occur.

Intuitively, it may seem odd that both head domains are in the post-power stroke state, since the ATP binding rate of this state is higher than that of pre-power stroke state.(Dunn et al., 2010; Oguchi et al., 2008) However, an optical trap study has suggested that when an external force is applied to the head domains, ATP binding rates dramatically slow.(Chuan et al., 2011) Even if ATP binding causes one head domain to detach and a small step to occur, myosin VI can return to its original adjacent binding state by taking a backward step to sustain its anchor function. We assume a backward force would enhance the anchor function by suppressing the ATPase activity of the myosin heads. Therefore, we argue that myosin VI restarts its stepping motion after releasing the backward force.

The dynamic anchor model for the myosin VI anchoring function

Finally, I propose a structural mechanism model for myosin VI anchoring, which does not depend on any biochemical regulation mechanism mentioned above (Figure 26). In this model, myosin VI switches its cellular function according to external load. When proper amount of load applied to myosin VI, it keeps the position taking "mark time". Once the load decreases, myosin VI can walk against the load until its stall force. On the other hand, the load increases over its stall force, the lever arms can not hold against the load and tilt backward which result in successive backward steps and the load decrement.

This model is a challenge to some previous studies described above section. However, most of all previous studies do not consider the adjacent binding state and forward tilts of lever arm domains which allow a head domain steps without tail domain movements. To clarify my model, further investigations are required.

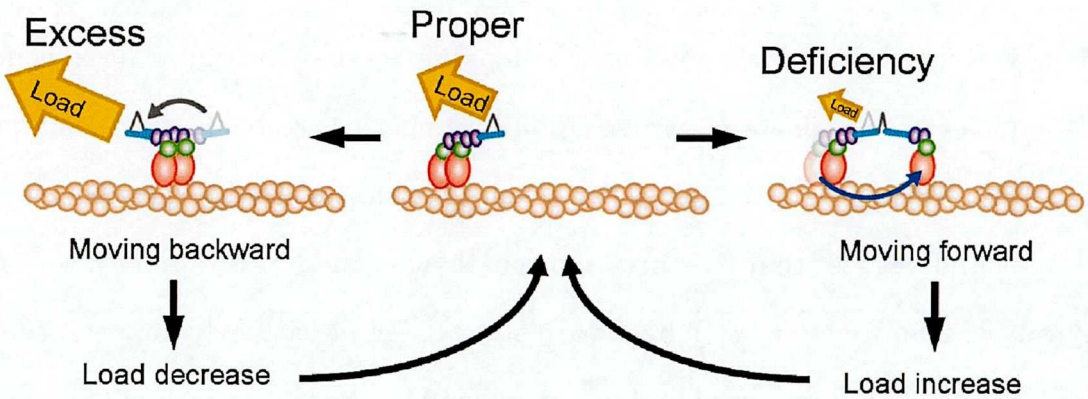

Figure 26. Model for Active anchoring of myosin VI.

A Model for Active anchoring of myosin VI. When proper amount of load applied to myosin VI, it keeps the position taking "mark time". Once the load decreases, myosin VI can walk against the load until its stall force. On the other hand, the load increases over its stall force, the lever arms can not hold against the load and tilt backward which result in successive backward steps and the load decrement.

4. Conclusion

In conclusion, we visualized single myosin VI stepping motion including both head domain steps and lever arm domain swings by observing the head and tail domains simultaneously. Our results revealed that two binding state of myosin VI enable its various step types and suggest that the three types of myosin VI steps are important for achieving myosin VI dual function, with backward steps being particularly important for the anchoring function. The step type is highly constrained by the forward tilt of the lever arm domains, as they permit only one backward step from the distant binding state and prohibit successive backward steps from the adjacent binding state. In turn, such constraints could regulate the myosin VI dual function.

Importantly, my results lead a possibility of a new working model for myosin VI cellular function, which does not only depends on biochemical regulations by external load but also structural constraints. I expect that like these structural constraints in myosin VI expand the automatic functionality of many proteins, not only motor proteins, and contribute to manage to complex system like a cell simpler.

5. Experimental section

Protein preparations: To create dimeric myosin VI constructs, the Human Myosin VI cDNA was truncated at Leu-989. This fragment included the motor domain, neck domain, and coiled-coil domain. To ensure myosin VI dimerization, the coiled-coil domain of chicken gizzard smooth muscle myosin encoding Val1450 - Ala1564 (Accession number X06546, gift from Dr. Ikebe) was appended at Leu989. For biotin and anti-His-antibody labeling, a HaloTag (DHA, Promega) fragment via a LRRRPTRPAMDPPSK linker and a 6 x His-tag fragment were attached at the N-terminal and C-terminal, respectively. Cloning, protein expression, and purification were performed as previously described (Nishikawa et al., 2010). Imidazole was removed by dialysis for Qdot585 anti-His-antibody conjugates labeling. Note that single labeled myosin VI with a Qdot probe at one of two head domains did not affect its motility, because almost all myosin VI binding to an actin filament were observed to move processively (Supplemental movie 1) and have intact motility (see also (Nishikawa et al., 2010)).

Myosin-Qdot conjugation: Qdot585 anti-His-antibody conjugates were synthesized using a Qdot585 antibody conjugation kit (Life Technologies, Invitrogen) and monoclonal anti-His-antibodies (Medical & Biological Laboratories, Japan). Q585 anti-His-antibody conjugates, Qdot525 streptavidin conjugates (Life Technologies, Invitrogen) and biotinylated myosin VI were mixed and incubated overnight on ice for simultaneous observation of the head and tail domains while Qdot585 streptavidin conjugates, Qdot525 streptavidin conjugates, and biotinylated myosin VI were incubated for the simultaneous observation of the two head domains.

Sample preparation for microscopy: A 10 µl volume microchamber was made by placing a

small coverslip (18 x 18 mm, No.1 Thickness, Matsunami, Japan) over a larger one (22 x 32 mm, No.1 Thickness, Matsunami, Japan) and using double-sided adhesive tape (50 μm thickness). Next, 1.5 mg/ml Actinin (Sigam-Aldrich) in assay buffer (AB: 20 mM HEPES-KOH (pH 7.8), 25 mM KCl, 5 mM MgCl2 and 1 mM EGTA) was adsorbed onto the glass surface, followed by a 3 min incubation, a 20 μl AB wash, and finally an injection of 2 μg/ml non-fluorescent phalloidin labeled actin filament solution in AB into the chamber. After another 3 min incubation and 20 μl AB wash, 5 mg/ml α-casein in AB was injected into the chamber. After a third 3 min incubation and 20 l AB wash, MB (AB plus an oxygen scavenger system, ATP regeneration system, and 20 μM ATP) including Qdot labeled myosin VI was flowed into the chamber and the chamber was sealed with nail polish.

Microscopy and image analysis: Qdot conjugated myosin VI movement was imaged using total internal reflection fluorescence microscopy (TIRFM). Qdot525 and 585 were excited by a 405 nm laser (Coherent, Compass405-50CW). The fluorescence was divided by a dual-view apparatus (Hamamatsu Photonics, A4313) equipped with dichroic mirrors (DML557nm, Asahi Spectra) and emission filters (FF01-520/35-25 and FF01-593/40-25, Semrock). The fluorescent images were captured with a back-illuminated EMCCD camera (Andor, DV887ECS-BV). Exported 14 bit data were imported into a custom written program with LabVIEW (National Instruments). The spot center for each frame was determined using a double Gaussian fit according to a published method(Thompson et al., 2002; Yildiz et al., 2003; Yildiz et al., 2004) and analyzed with SHREC. Accuracy of the spot center detection was 2.0 nm. Images of double-labeled myosin were obtained and analyzed in accordance with SHREC. The accuracy of the control grid function was maintained for stable myosin VI measurements.(Nishikawa et al., 2010) All steps were

detected by eye.

6. References

Ali, M.Y., Homma, K., Iwane, A.H., Adachi, K., Itoh, H., Kinosita, K., Jr., Yanagida, T., and Ikebe, M. (2004). Unconstrained steps of myosin VI appear longest among known molecular motors. Biophys. J. 86, 3804–3810.

Altman, D., Goswami, D., Hasson, T., Spudich, J.A., and Mayor, S. (2007). Precise positioning of myosin VI on endocytic vesicles in vivo. PLoS Biol. 5, e210.

Altman, D., Sweeney, H.L., and Spudich, J.A. (2004). The mechanism of myosin VI translocation and its load-induced anchoring. Cell 116, 737–749.

Bahloul, A., Chevreux, G., Wells, A.L., Martin, D., Nolt, J., Yang, Z., Chen, L.Q., Potier, N., Van Dorsselaer, A., Rosenfeld, S., et al. (2004). The unique insert in myosin VI is a structural calcium-calmodulin binding site. Proc. Natl. Acad. Sci. USA 101, 4787–4792.

Balci, H., Ha, T., Sweeney, H.L., and Selvin, P.R. (2005). Interhead distance measurements in myosin VI via SHRImP support a simplified hand-overhand model. Biophys. J. 89, 413–417.

Bryant, Z., Altman, D., and Spudich, J.A. (2007). The power stroke of myosin VI and the basis of reverse directionality. Proc. Natl. Acad. Sci. USA 104, 772–777.

Chuan, P., Spudich, J.A., and Dunn, A.R. (2011). Robust mechanosensing and tension

generation by myosin VI. J Mol Biol 405, 105-112.

Churchman, L.S., Okten, Z., Rock, R.S., Dawson, J.F., and Spudich, J.A. (2005). Single molecule high-resolution colocalization of Cy3 and Cy5 attached to macromolecules measures intramolecular distances through time. Proc. Natl. Acad. Sci. USA 102, 1419–1423.

Churchman, L.S., and Spudich, J.A. (2007). In Colocalization of Fluorescent Probes: Accurate and Precise Registration with Nanometer Resolution. Single-molecule techniques: a Laboratory Manual, P.R. Selvin and T.J. Ha, eds., pp. 73–84.

De La Cruz, E.M., Ostap, E.M., and Sweeney, H.L. (2001). Kinetic mechanism and regulation of myosin VI. J. Biol. Chem. 276, 32373–32381.

Dunn, A.R., Chuan, P., Bryant, Z., and Spudich, J.A. (2010). Contribution of the myosin VI tail domain to processive stepping and intramolecular tension sensing. Proceedings of the National Academy of Sciences 107, 7746-7750.

Dunn, A.R., and Spudich, J.A. (2007). Dynamics of the unbound head during myosin V processive translocation. Nat. Struct. Mol. Biol. 14, 246–248.

Elting, M.W., Bryant, Z., Liao, J.-C., and Spudich, J.A. (2011). Detailed Tuning of Structure and Intramolecular Communication Are Dispensable for Processive Motion of Myosin VI. Biophysical Journal 100, 430-439.

Funatsu, T., Harada, Y., Tokunaga, M., Saito, K., and Yanagida, T. (1995). Imaging of single fluorescent molecules and individual ATP turnovers by single myosin molecules in aqueous solution. Nature 374, 555–559.

Gebhardt, J.C., Clemen, A.E., Jaud, J., and Rief, M. (2006). Myosin-V is a mechanical ratchet. Proc Natl Acad Sci U S A 103, 8680-8685.

Goldman, Y.E. (1987). Kinetics of the Actomyosin ATPase in Muscle Fibers. A Rev Physiol. 49, 637–654.

Harada, Y., Sakurada, K., Aoki, T., Thomas, D.D., and Yanagida, T. (1990). Mechanochemical coupling in actomyosin energy transduction studied by in vitro movement assay. J. Mol. Biol. 216, 49–68.

Iwaki, M., Iwane, A.H., Shimokawa, T., Cooke, R., and Yanagida, T. (2009). Brownian search-and-catch mechanism for myosin-VI steps. Nat. Chem. Biol. 5, 403–405.

Kinosita, K., Jr., Itoh, H., Ishiwata, S., Hirano, K., Nishizaka, T., and Hayakawa, T. (1991). Dual-view microscopy with a single camera: real-time imaging of molecular orientations and calcium. J. Cell Biol. 115, 67–73.

Lan, G., and Sun, S.X. (2006). Flexible light-chain and helical structure of F-actin explain the movement and step size of myosin-VI. Biophys. J. 91, 4002–4013.

Menetrey, J., Bahloul, A., Wells, A.L., Yengo, C.M., Morris, C.A., Sweeney, H.L., and Houdusse, A. (2005). The structure of the myosin VI motor reveals the mechanism of directionality reversal. Nature 435, 779–785.

Menetrey, J., Llinas, P., Cicolari, J., Squires, G., Liu, X., Li, A., Sweeney, H.L., and Houdusse, A. (2008). The post-rigor structure of myosin VI and implications for the recovery stroke. EMBO J. 27, 244–252.

Mukherjea, M., Llinas, P., Kim, H., Travaglia, M., Safer, D., Menetrey, J., Franzini-Armstrong, C., Selvin, P.R., Houdusse, A., and Sweeney, H.L. (2009). Myosin VI dimerization triggers an unfolding of a three-helix bundle in order to extend its reach. Mol. Cell 35, 305–315.

Nishikawa, S., Homma, K., Komori, Y., Iwaki, M., Wazawa, T., Hikikoshi Iwane, A., Saito, J., Ikebe, R., Katayama, E., Yanagida, T., et al. (2002). Class VI myosin moves processively along actin filaments backward with large steps. Biochem. Biophys. Res. Commun. 290, 311–317.

Oguchi, Y., Mikhailenko, S.V., Ohki, T., Olivares, A.O., De La Cruz, E.M., and Ishiwata, S. (2008). Load-dependent ADP binding to myosins V and VI: Implications for subunit coordination and function. Proceedings of the National Academy of Sciences 105, 7714-7719.

Okten, Z., Churchman, L.S., Rock, R.S., and Spudich, J.A. (2004). Myosin VI walks hand-over-hand along actin. Nat. Struct. Mol. Biol. 11, 884–887.

Park, H., Li, A., Chen, L.Q., Houdusse, A., Selvin, P.R., and Sweeney, H.L. (2007). The unique insert at the end of the myosin VI motor is the sole determinant of directionality. Proc. Natl. Acad. Sci. USA 104, 778–783.

Park, H., Ramamurthy, B., Travaglia, M., Safer, D., Chen, L.Q., Franzini-Armstrong, C., Selvin, P.R., and Sweeney, H.L. (2006). Full-length myosin VI dimerizes and moves processively along actin filaments upon monomer clustering. Mol. Cell 21, 331–336.

Phichith, D., Travaglia, M., Yang, Z., Liu, X., Zong, A.B., Safer, D., and Sweeney, H.L. (2009). Cargo binding induces dimerization of myosin VI. Proc. Natl. Acad. Sci. USA 106, 17320–17324.

Purcell, T.J., Sweeney, H.L., and Spudich, J.A. (2005). A force-dependent state controls the coordination of processive myosin V. Proc Natl Acad Sci U S A 102, 13873-13878.

Reifenberger, J.G., Toprak, E., Kim, H., Safer, D., Sweeney, H.L., and Selvin, P.R. (2009). Myosin VI undergoes a 180 degrees power stroke implying an uncoupling of the front lever arm. Proc. Natl. Acad. Sci. USA 106, 18255–18260.

Rock, R.S., Ramamurthy, B., Dunn, A.R., Beccafico, S., Rami, B.R., Morris, C., Spink, B.J., Franzini-Armstrong, C., Spudich, J.A., and Sweeney, H.L. (2005). A flexible domain is

essential for the large step size and processivity of myosin VI. Mol. Cell 17, 603–609.

Rock, R.S., Rice, S.E., Wells, A.L., Purcell, T.J., Spudich, J.A., and Sweeney, H.L. (2001). Myosin VI is a processive motor with a large step size. Proc. Natl. Acad. Sci. USA 98, 13655–13659.

Shiroguchi, K., and Kinosita, K., Jr. (2007). Myosin V walks by lever action and Brownian motion. Science 316, 1208–1212.

Sivaramakrishnan, S., and Spudich, J.A. (2009). Coupled myosin VI motors facilitate unidirectional movement on an F-actin network. J. Cell Biol. 187, 53–60.

Spink, B.J., Sivaramakrishnan, S., Lipfert, J., Doniach, S., and Spudich, J.A. (2008). Long single a-helical tail domains bridge the gap between structure and function of myosin VI. Nat. Struct. Mol. Biol. 15, 591–597.

Spudich, J.A., and Sivaramakrishnan, S. (2010). Myosin VI: an innovative motor that challenged the swinging lever arm hypothesis. Nat. Rev. Mol. Cell Biol. 11, 128–137.

Sun, Y., Schroeder, H.W., 3rd, Beausang, J.F., Homma, K., Ikebe, M., and Goldman, Y.E. (2007). Myosin VI walks "wiggly" on actin with large and variable tilting. Mol. Cell 28, 954–964.

Sweeney, H.L., and Houdusse, A. (2007). What can myosin VI do in cells? Curr. Opin. Cell

Biol. 19, 57–66.

Taniguchi, Y., Nishiyama, M., Ishii, Y., and Yanagida, T. (2005). Entropy rectifies the Brownian steps of kinesin. Nat. Chem. Biol. 1, 342–347.

Thompson, R.E., Larson, D.R., and Webb, W.W. (2002). Precise nanometer localization analysis for individual fluorescent probes. Biophys. J. 82, 2775–2783.

Tokunaga, M., Kitamura, K., Saito, K., Iwane, A.H., and Yanagida, T. (1997). Single molecule imaging of fluorophores and enzymatic reactions achieved by objective-type total internal reflection fluorescence microscopy. Biochem. Biophys. Res. Commun. 235, 47–53.

Ueno, H., Nishikawa, S., Iino, R., Tabata, K.V., Sakakibara, S., Yanagida, T., and Noji, H. (2010). Simple Dark-Field Microscopy with Nanometer Spatial Precision and Microsecond Temporal Resolution. Biophys. J. 98, 2014–2023.

Vale, R.D., Funatsu, T., Pierce, D.W., Romberg, L., Harada, Y., and Yanagida, T. (1996). Direct observation of single kinesin molecules moving along microtubules. Nature 380, 451–453.

Warshaw, D.M., Kennedy, G.G., Work, S.S., Krementsova, E.B., Beck, S., and Trybus, K.M. (2005). Differential Labeling of Myosin V Heads with Quantum Dots Allows Direct Visualization of Hand-Over-Hand Processivity. Biophys. J. 88, L30–L32.

Wells, A.L., Lin, A.W., Chen, L.Q., Safer, D., Cain, S.M., Hasson, T., Carragher, B.O., Milligan, R.A., and Sweeney, H.L. (1999). Myosin VI is an actin-based motor that moves backwards. Nature 401, 505–508.

Yildiz, A., Forkey, J.N., McKinney, S.A., Ha, T., Goldman, Y.E., and Selvin, P.R. (2003). Myosin V walks hand-over-hand: single fluorophore imaging with 1.5-nm localization. Science 300, 2061–2065.

Yildiz, A., Park, H., Safer, D., Yang, Z., Chen, L.Q., Selvin, P.R., and Sweeney, H.L. (2004). Myosin VI steps via a hand-over-hand mechanism with its lever arm undergoing fluctuations when attached to actin. J. Biol. Chem. 279, 37223–37226.

7. Acknowledges

This study was supported by QBiC, RIKEN, Japan, the Global COE program "System Dynamics of Biological Function", and Sekisui funding, Japan. I am also supported by the Junior Research Associate program, Riken, Japan.

I thank members of QBiC for valuable discussion. I especially thank Professor Toshio Yanagida and assistant professor Tomotaka Komori.

I also thank Prof. Ogura, Prof. Yagi and Prof. Yamamoto for warm acceptance of a committee post for my judging committee.

8. Presentation List

Treatises

*S. Nishikawa, * I. Arimoto, **K. Ikezaki**, M. Sugawa, H. Ueno, T. Komori, A. H. Iwane, and T. Yanagida *equal contribution, "Switch between large hand-over-hand and small inchworm-like steps in myosin VI", **Cell**, September 17, 2010, 142, 879–888

K. Ikezaki, T. Komori, M. Sugawa, Y. Arai, S. Nishikawa, A. H. Iwane and T. Yanagida, "Simultaneous Observation of the Lever Arm and Head Explains Myosin VI Dual Function", **Small**, July 9, 2012

Oral presentations

K. Ikezaki, T. Komori, M. Sugawa, Y. Arai, S. Nishikawa, A. H. Iwane and T. Yanagida, "Contribution of the lever arm to myosin VI's dual function as a transporter and an anchor.", **日本生物物理学会第 49 回年会**、兵庫県立大学、2011 年 9 月

池崎圭吾、須河光弘、西川宗、小森智貴、岩根敦子、柳田敏雄, "ミオシン 6 の SHREC 計測", **2010 年 生体運動研究合同班会議** 、中央大学後楽園キャンパス、2010 年 1 月

池崎圭吾、小森智貴、須河光弘、新井由之、西川宗、岩根敦子、柳田敏雄, "ミオシン 6 の 2 つの生理的機能発現のための分子機構", **2012 年 生体運動研究合同班会議** 、筑波大学、2012 年 1 月

Poster presentations

K. Ikezaki, T. Komori, M. Sugawa, Y. Arai, S. Nishikawa, A. H. Iwane and T. Yanagida, " The adjacent binding state enables Myosin VI dual function", **Biophysical Society 56th Annual Meeting**, San Diego, California, February, 2012.

K. Ikezaki, T. Komori, M. Sugawa, S. Nishikawa, A. H. Iwane and T. Yanagida, "The tail domain of myosin-VI ensures the directed processive movement.", **Biophysical Society 55th Annual Meeting**, Baltimore, Maryland, March, 2011.

K. Ikezaki, T. Komori, M. Sugawa, S. Nishikawa, A. H. Iwane and T. Yanagida, "SHREC measurement of myosin-VI stepping motion", **Biophysical Society 54th Annual Meeting**, San Francisco, California, February, 2010.

K. Ikezaki, T. Komori, M. Sugawa, S. Nishikawa, A. H. Iwane, T. Yanagida, "The regulation mechanism for myosin VI steps.", **Structural Biology Research Center International Symposium**, Nagoya, November, 2010.

K. Ikezaki, M. Sugawa, S. Nishikawa, T. Komori, A. H. Iwane, T. Yanagida, "SHREC measurement of myosin-VI stepping motion", **RIKEN Quantitative Biology Center Kick-off meeting**, Osaka, October 2010.

池崎圭吾、小森智貴、須河光弘、西川宗、岩根敦子、柳田敏雄, "ミオシン6 の歩幅の調整機

構", 日本生物物理学会第 48 回年会、東北大学、2010 年 9 月

池崎圭吾、須河光弘、西川宗、岩根敦子、柳田敏雄, "ミオシン 6 の SHREC 計測", 日本生物物理学会第 47 回年会、2P-131、アスティとくしま、2009 年 10 月

Fin.